Smart Structures and Systems, *Vol. 28, No. 4 (2021) 515-533*
https://doi.org/10.12989/sss.2021.28.4.515

Dynamics of perforated higher order nanobeams subject to moving load using the nonlocal strain gradient theory

Alaa A. Abdelrahman [1], Ismail Esen [2], Cevat Özarpa [2],
Ramy Shaltout [3,4], Mohamed A. Eltaher[*5,7] and Amr E. Assie [6,7]

[1] *Mechanical Design & Production Department, Faculty of Engineering, Zagazig University, P.O. Box 44519, Zagazig, Egypt*
[2] *Department of Mechanical Engineering, Karabuk University, Karabuk, Turkey*
[3] *Mechanical Power Department, Faculty of Engineering, Zagazig University, P.O. Box 44519, Zagazig, Egypt*
[4] *Transportation Research Centre- German University in Cairo (GUC), Egypt*
[5] *Mechanical Engineering Department, Faculty of Engineering, King Abdulaziz University, P.O. Box 80204, Jeddah, Saudi Arabia*
[6] *Mechanical Engineering Department, Faculty of Engineering, Jazan University, P.O. Box 45142, Jazan, Kingdom of Saudi Arabia*
[7] *Mechanical Design & Production Department, Faculty of Engineering, Zagazig University, P.O. Box 44519, Zagazig, Egypt*

(*Received December 31, 2020, Revised May 13, 2021, Accepted May 17, 2021*)

Abstract. The goal of this manuscript is to develop a nonclassical size dependent model to study and analyze the dynamic behaviour of the perforated Reddy nanobeam under moving load including the length scale and microstructure effects, that not considered before. The kinematic assumption of the third order shear deformation beam theory in conjunction with modified continuum constitutive equation of nonlocal strain gradient (NLSG) elasticity are proposed to derive the equation of motion of nanobeam included size scale (nonlocal) and microstructure (strain gradient) effects. Mathematical expressions for the equivalent geometrical parameters due to the perforation process of regular squared pattern are developed. Based on the virtual work principle, the governing equations of motion of perforated Reddy nanobeams are derived. Based on Navier's approach, an analytical solution procedure is developed to obtain free and forced vibration response under moving load. The developed methodology is verified and checked with previous works. Impacts of perforation, moving load velocity, microstructure parameter and nonlocal size scale effects on the dynamic and vibration responses of perforated Reddy nanobeam structures have been investigated in a wide context. The obtained results are supportive for the design of MEMS/NEMS structures such as frequency filters, resonators, relay switches, accelerometers, and mass flow sensors, with perforation.

Keywords: analytical solution; dynamic analysis of moving load; higher order shear deformation; nonlocal strain gradient theory; perforated nanobeam

1. Introduction

The increase of using nanotechnology and nanoscale materials have led to expanding the interest in micromechanical modeling, Esen *et al*. (2020). It is noted in studying of nanoscale structures that, there is an inconsistency between experimental and classical continuum mechanics and classic theory cannot foretelling the response of nanostructures correctly. Thus, many scientists and researchers developed modified continuum theories containing length scale effect to define response of nano systems precisely, such as, nonlocal elasticity (Eringen 1983, Bouafia *et al*. 2017, Mouffoki *et al*. 2017), couple stress theory (Koiter 1964), strain gradient theory (Mindlin 1965, Ma *et al*. 2008), surface elasticity theory (Gurtin and Murdoch 1978, Mahmoud *et al*. 2012, Shen *et al*. 2017), energy equivalent method (Wu *et al*. 2006, Mohamed *et al*. 2019, 2020), doublet mechanics (Ferrari *et al*. 1997, Eltaher and Mohamed 2020, Eltaher *et al*. 2020a).

Based on nanomechics analysis, Li *et al*. (2015a, b) exploited semi-continuum model based on Euler beam and nonlocal elasticity models to investigate the free vibration and natural frequencies of extreme-thin nanobeam. Yaylı (2015, 2016) exploited gradient elasticity theory and surface energy to present the size effect on the buckling response of microbeams restrained by translational and rotational springs and rested on elastic media. Akbaş (2016) studied the forced vibration response of viscoelastic modified couple stress nanobeams embedded in an elastic medium. Eltaher *et al*. (2016) predicted the sensitivity of CNTs in measuring particles with zeptogram mass using nonlocal elasticity and finite element method. Shen and Li (2017) developed a modified semi-continuum model based on Euler beam and nonlocal elasticity models to investigate the bending deformation of extreme-thin nanobeam. Yaylı (2018a, b) illustrated the torsional frequencies of restrained nanotubes embedded in an elastic medium via nonlocal elasticity and modified couple stress theory. Yaylı (2018c, 2020) derived an efficient solution method to study a free longitudinal vibration of CNTs and FG nanorods via a hardening nonlocal approach. Balubaid *et al*. (2019) illustrated the vibration response of nonlocal FG nanoplate by using the two variables integral refined plate theory.

*Corresponding author, Professor,
E-mail: meltaher@kau.edu.sa; mmeltaher@zu.edu.eg

ISSN: 1738-1584 (Print), 1738-1991 (Online)

Boutaleb *et al*. (2019) analyzed the vibration behavior of FG nonlocal nanoplates based on the quasi-3D high shear deformation theory. Berghouti *et al*. (2019) presented the vibration behavior of FG porous nonlocal nanobeams using nth-order shear deformation theory. Semmah *et al*. (2019) exploited the nonlocal elasticity with first order shear theory to study the thermal buckling of zigzag single-walled boron nitride rested on Winkler elastic foundation. Alimirzaei *et al*. (2019) developed a finite element model to study the nonlinear bending, buckling and vibration behaviours of viscoelastic imperfect micro-composite beam under electro-magnetic environments. Based on integral first-order shear deformation theory, Draiche *et al*. (2019) developed an analytical model to envisage the bending deflection of laminated reinforced composite plates subjected to sinusoidal and uniform loads. Hussain *et al*. (2019) and Asghar *et al*. (2020) evaluated the natural frequencies of chiral and zigzag double-walled CNTs in the frame of Donnell shell model and Eringen's nonlocal elasticity theory. Uzun *et al*. (2020) developed a finite element model including modified couple stress and Rayleigh beam theory to present vibration of cantilever CNT based sensor. Matouk *et al*. (2020) studied the hygro-thermal vibration of FG nanobeam using nonlocal integral Timoshenko beam theory. Bourada *et al*. (2020) and Bousahla *et al*. (2020) illustrated the dynamic and buckling stability of SWCNT reinforced concrete beam rested on elastic-foundation. Rouabhia *et al*. (2020) and Bellal *et al*. (2020) investigated the critical buckling load of a single-layered graphene sheet rested on visco-Pasternak's medium by using nonlocal integral elasticity and first shear deformation theory. Yao *et al*. (2020) investigated the vibration response and wave propagation of FG nonlocal Timoshenko microbeams with an axial motion. Almitani *et al*. (2020a) studied the free vibration, frequency response and modal participation factors of perforated multilayer microbeam structures using finite element method. Abo-Bakr (2020b, 2021) evaluated the optimized weight and critical buckling load of size dependent modified couple stress microbeam. Alazwari *et al*. (2021) included the modified couple stress and the surface elasticity model to present the size influence on the deflection of perforated nanobeam structure. Esen *et al*. (2021b) derived a model capable to predict a vibrational behavior of FG cracked nonlocal microbeam rested on elastic foundation and exposed to thermal and magnetic fields. Yaylı *et al*. (2021) used strain gradient elasticity to predict the size-dependent stability of nanobeams under axial loading is investigated by strain gradient elasticity

Based on nonlocal strain gradient theory (NSGT), Ebrahimi *et al*. (Ebrahimi and Shafiei 2016, Ebrahimi and Shaghaghi 2016, Ebrahimi *et al*. 2017) studied thermal effects on wave propagation of quasi-3D FG nanobeams and nanoplate. Arani *et al*. (2017, 2018) forecasted the influence of electric, magnetic and thermal environments on wave propagation of NLSG nanobeam and nanoplates. Lu *et al*. (2018) presented nonlocal and material length scale parameters, and surface energy effects on buckling stability of nanoplates using analytical procedure. Li *et al*. (2019) shown that an interval for the scale parameter can be found on the basis of the nonlocal softening physical mechanism, in which the equivalent stiffness of nano-structures is weakened than that predicted by the classical continuum theory. Karami *et al*. (2019a, b) developed refined mathematical model to investigate the buckling stability of anisotropic nanoplates and nanoshell subjected to magnetic environments. Shen *et al*. (2019) illustrated new observations on dynamic response of microtubules under axial load, thermal load and variable transverse load based on nonlocal strain gradient theory. Daikh *et al*. (2019, 2020a, b) examined the thermal stability and dynamic behavior of sandwich nonlocal strain gradient nanoplates resting on a Kerr foundation. Daikh *et al*. (2020b) established a nonlocal strain gradient mathematical model based to predict the bending response of CNTRC nanobeams. Abo-Bakr *et al*. (2020a) studied the influence of surface and stiffening on the Pull-in stability of FG nanobeams actuated by electrical field. Li and Li (2020) explored the size impact on vibration of rotating double-tapered cantilever Timoshenko nanobeam.

Eltaher and Abdelrahman (2020) and Almitani *et al*. (2020b) presented the influence of surface energy and perforation on the bending and static stability of nanobeam by incorporated the surface properties. Abdelrahman and Eltaher (2020) studied bending and buckling responses of perforated nanobeams including surface energy for different beams theories. She (2020) studied a wave propagation of FG nanoplates reinforced with graphene nanoplatelets and rested on elastic foundations. Eltaher and Mohamed (2020b) and Hamed *et al*. (2020) investigated the mechanical responses of perforated nanobeam by using nonlocal elasticity of Eringen. Eltaher *et al*. (2020a, b, c) included nonlocal elasticity and surface energy properties to illustrate the size influence on the bending and vibration behaviors of perforated nanobeam. Shen *et al*. (2020) studied analytically the stability and vibration of FG nonlocal strain gradient nanoplates with axial motion. Daikh *et al*. (2021a) evaluated of the critical buckling load of of CNTRC Curved sandwich nanobeams under a thermal load. Daikh *et al*. (2021b) studied the bending deflection and stresses of sandwich FG quasi 3D hyperbolic nanoplates rested on variable elastic foundation. She *et al*. (2021) predicted the resonance of composite curved strain gradient microbeams reinforced with graphene nanoplatelets by using Navier solution procedure. Lu *et al*. (2021) studied the size-dependent postbuckling of graphene reinforced composite curved microtubes. Esen *et al*. (2021d) studied static and dynamic stability of FG nanobeams subjected to magnetic and thermal environments.

Recognizing and influencing the motion of nanoparticles is critical for micro- and nanoassembly, microfluidics, including biological and colloidal science applications, chemical mechanical polishing, and xerographic processes, Eglin *et al*. (2006). Such as, nanotube and nanobeams may be used to transport drug materials into targeted nano-sized molecules to change the behaviour of cancer cells, Roudbari *et al*. (2020). Therefore, understanding the mechanism of mass transport and the dynamic behavior of microbeams under such loadings would be of great importance for the optimal design of

beam-type microstructures in the future, Şimşek (2010).

Pourseifi *et al*. (2015) considered vibration control of nonlocal nanotube under a moving nanoparticle by using classical optimal control algorithm. Bourouina *et al*. (2016) derived an analytical solution to evaluate nonlocal resonance frequencies of perforated nanobeams under temperature-induced loads. Ghadiri *et al*. (2017) predicted a steady-state response of nanobeam under moving concentrated load and rested on a viscoelastic. Hashemi and Khaniki (2018) studied the response of multiple nanobeam system under a moving nanoparticle using Eringen's nonlocal theory. Abdelrahman *et al*. (2019) and Almitani *et al*. (2019) used Galerkin-Laplace technique to study the forced response of perforated Euler and Timoshenko beam. Cao *et al*. (2019) studied magnetic-tunable sound absorber based on micro-perforated magnetorheological elastomer. Esen (2019a, b) studied the thermoelastic dynamic response of FG beam resting on elastic foundation and subjected to moving accelerating mass by using finite element method. Özarpa and Esen (2020) and Esen (2020) studied the size effect using both modified couple stress and nonlocal strain gradient on the dynamic response of nanobeam under moving loads by using FEM. Almitani *et al*. (2020b) presented the impact of perforation on the free vibration and frequency response of multilayer beam using finite element method. Kim *et al*. (2020) investigated sound transmission loss of multi-layered infinite micro-perforated plates. Hamidi *et al*. (2020) studied the vibration forced response of nonlocal strain gradient nanobeam under distributed moving axial force. Esen *et al*. (2020) exploited modified couple stress theory and Timoshenko theory to study the dynamic response of perforated microbeams under moving loads by using finite element method. Abdelrahman *et al*. (2021) developed finite element model based on nonlocal strain gradient and Timoshenko beam to investigate the dynamic response of the perforated nanobeam under moving mass. Esen *et al*. (2021a) exploited Newmark time integration to studied dynamic behavior of symmetric and sigmoid FG Timoshenko beam rested on elastic foundation under moving mass. Esen *et al*. (2021c) predicted the dynamic behavior of composite nanobeams reinforced by CNTs under a moving mass investigated. Assie *et al*. (2021) studied the vibration behavior of perforated thick beam under moving load using Ritz method.

Based on literature and author's information, the dynamic vibration response of perforated higher order nonlocal strain gradient nanobeam under moving load, has not been studied. Thus, the current point will be considered comprehensively through this study. The manuscript is structured as following: the problem formulation with constitutive equations are presented through section 2. The next section presented the analytical solution procedure. Verification of the present model with previously published work has been illustrated in section 4. The numerical results and parametric studies have been developed and discussed in section 5. The main conclusions and highlighted results are presented in section 6.

2. Problem formulation

2.1 Effective characteristics of perforated beams

Consider a perforated beam with regular squared holes as shown in Fig. 1, where the x-axis passes through the midpoint of the beam. The filling ratio of the perforated beam structure can be given by, Abdelrahman *et al*. (2020a, b)

$$\alpha = \frac{t_s}{l_s} \qquad 0 \le \alpha \le 1, \tag{1}$$

where l_s and t_s refer to the spatial period and to the period length; respectively. The equivalent nondimensional bending and shear stiffnesses $\frac{[EI]_{eq}}{[EI]_s}$ and $\frac{[\mu A]_{eq}}{[EA]_s}$ can be expressed as, Luschi and Pieri (2014)

$$\frac{[EI]_{eq}}{[EI]_s} = \left\{ \begin{matrix} \dfrac{\alpha(N+1)(N^2+2N+\alpha^2)}{(1-\alpha^2+\alpha^3)N^3+3\alpha N^2} \\ +(3+2\alpha-3\alpha^2+\alpha^3)\alpha^2 N+\alpha^3 \end{matrix} \right\} \tag{2a}$$

$$\frac{[\mu A]_{eq}}{[EA]_s} = \left\{ \frac{\alpha^3(N+1)}{2N} \right\} \tag{2b}$$

with E is the Young's modulus and μ is the rigidity modulus of the solid beam elastic material while I is the second moment of area and A is the cross sectioanl area of the solid beam, N is the number of holes throughout the cross section, α is the filling ratio.

The equivalent mass per unit length and the equivalent rotary inertia of perforated beam can be expressed as, Eltaher *et al*. (2018a, b)

$$\frac{[\rho A]_{eq}}{[\rho A]_s} = \left\{ \frac{[1-N(\alpha-2)]\alpha}{N+\alpha} \right\} \tag{3a}$$

$$\frac{[\rho I]_{eq}}{[\rho I]_s} = \left\{ \frac{\alpha[(2-\alpha)N^3+3N^2-2(\alpha-3)(\alpha^2-\alpha+1)N+\alpha^2+1]}{(N+\alpha)^3} \right\} \tag{3b}$$

where, ρ and A are the mass density and the cross sectional area of the solid beam; respectively.

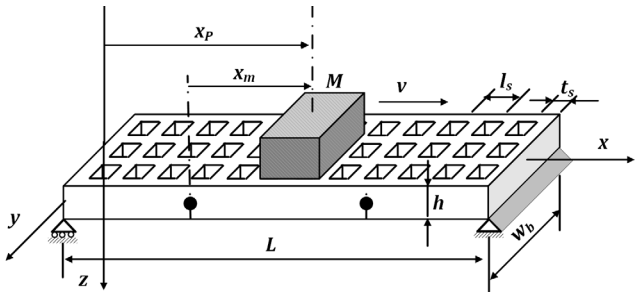

Fig. 1 Geometry of a regularly squared perforated beam

2.2 Nonlocal strain gradient elasticity

Based on Eringen's non-local elasticity theory, stress at a point is a function of stress at that point as well as that elastic body. This theory can predict the softening of the structure according to non-local dimension effects. In the other hand, strain gradient theory, which is a higher order theory of elasticity, considers only the stiffness-enhancing effect. As a result, Eringen's non-local flexibility and strain gradient theories define two completely different physical properties of an elastic body. This allows us to use the nonlocal strain gradient theory (NSGT), which takes advantage of both theories from a single point of view. Based on non-local strain gradient theory, integral equations are as follows, Lim *et al*. (2015)

$$\sigma = \int_V \alpha_0(\boldsymbol{x}', \boldsymbol{x}, e_0 a)\boldsymbol{C} : \varepsilon'(\boldsymbol{x}')dV'. \tag{4}$$

$$\sigma^{(1)} = l^2 \int_V \alpha_1(\boldsymbol{x}', \boldsymbol{x}, e_1 a)\boldsymbol{C} : \nabla\varepsilon'(\boldsymbol{x}')dV'. \tag{5}$$

Here ∇ is the Laplacian operator, σ, represents the classical stress tensor at point x, while $\sigma^{(1)}$ is the higher-order stress tensor, $\boldsymbol{C}$ is the fourth-order material constant, ε is the classical strain tensor and $\nabla\varepsilon$ is the strain gradient tensor. And l, α_0 and α_1, are the material length scale parameter, classical and higher-order nonlocal kernel functions, respectively. $e_0 a$ and $e_1 a$ represent nonlocality coefficients, where e_0 and e_1 are material constants and a is related to geometrical characteristics of C−C bonds between molecules. And ":" symbolises double-dot product of tensors.

In nonlocality modelling, there are different non-local kernel functions (α_0) with which, Eq. (4) can be reduced to other gradient theories such as stress gradient or pure strain gradient theories.

Total normal and shear stress components, σ^t and τ^t of NSGT is (Lim *et al*. 2015, Farajpour and Rastgoo 2017)

$$\sigma^t = \sigma - \nabla\sigma^{(1)}. \tag{6a}$$

$$\tau^t = \tau - \nabla\tau^{(1)}. \tag{6b}$$

where σ and τ are respectively the normal and shear stress components, $\sigma^{(1)}$ and $\tau^{(1)}$ are the higher order normal and shear stress components, and ∇ is the one dimensional differential operator, $\nabla = \frac{\partial}{\partial x}$.

It is very difficult to solve the integral (6), thus a simplified differential form equation will be used. Assuming $e = e_0 = e_1$ and the nonlocal functions $\alpha_0(x', x, e_0 a)$ and $\alpha_1(x', x, e_1 a)$ satisfy the conditions of Eringen (1983), thus, the linear differential operator can be used for the nonlocal functions, hence

$$\left[1 - (ea)^2 \nabla^2\right] \sigma = \mathbf{C} : \varepsilon. \tag{7}$$

$$\left[1 - (ea)^2 \nabla^2\right] \sigma^{(1)} = l^2 \mathbf{C} : \nabla\varepsilon \tag{8}$$

and the total stress can be reduced as

$$\left[1 - (ea)^2 \nabla^2\right] \sigma^t = \mathbf{C} : \varepsilon - l^2 \nabla\mathbf{C} : \nabla\varepsilon. \tag{9}$$

where, ∇ is the Laplacian operator, σ represents the classical Cauchy stress tensor at point x, while $\sigma^{(1)}$ is the higher order stress tensor, C is the fourth-order material constant, ε is the classical infinitesimal strain tensor and $\nabla\varepsilon$ is the strain gradient tensor. And l is the material length scale parameter. ea represents the non-locality coefficient, where e is material constant and a is related to geometrical characteristics parameter. In the case of a beam structure, the general constructive relationship can be further simplified by ignoring dimension-dependent behaviour in width and thickness directions (Lim *et al*. 2015, Li and Hu 2016a, Li *et al*. 2016). Hence

$$\left[1 - (ea)^2 \nabla^2\right] \sigma_{xx}^t = \left[1 - l^2\nabla^2\right] E\varepsilon_{xx}, \tag{10a}$$

$$\left[1 - (ea)^2 \nabla^2\right] \sigma_{xz}^t = \frac{1}{2}\left[1 - l^2\nabla^2\right] G\varepsilon_{xz}. \tag{10b}$$

where E and G are the elasticity and shear moduli, σ_{xx}^t and σ_{xz}^t are the axial normal and shear stresses, ε_{xx} and ε_{xz} are the axial and shear strains. Using the Eqs. (10), the constitutive equation of nonlocal continuum theory of Eringen (1983) can be obtained by setting $l = 0$, and that of strain gradient theory by setting $ea = 0$. It is reported by (Lim *et al*. 2015, Li *et al*. 2016), the general constitutive Eqs. (10a) and (10b) can practically describe size-dependent phenomena since the simulation results of molecular dynamics and the results of nonlocal strain gradient theory are in a good agreement.

2.3 Higher order nanobeam with nonlocal strain gradient theory

Displacement field

According to the Reddy third order shear deformation beam theory, the displacement field can be expressed as, Reddy (2017) and Esen *et al*. (2021c)

$$u_x(x, z, t) = u(x) - z\frac{\partial w}{\partial x} + \Phi(z)\left(\frac{\partial w}{\partial x} - \varphi\right). \tag{11a}$$

$$u_z(x, z, t) = w(x), \tag{11b}$$

$$\text{with} \quad \Phi = z\left(1 - \frac{4z^2}{3h^2}\right) \tag{11c}$$

where u and w are the longitudinal and the transverse displacements, φ is the rotational of the cross section at each point of the neutral axis.

Kinematic and kinetic relations

Based on the defined displacement field in Eqs. (11), the nonzero strain components of the Reddy beam model are defined as follows

$$\varepsilon_{xx} = \frac{\partial u_x}{\partial x} = \varepsilon_{xx}^{(0)} + z\varepsilon_{xx}^{(1)} + z^3\varepsilon_{xx}^{(3)} \tag{12a}$$

$$\varepsilon_{xz} = \frac{1}{2}\left(\frac{\partial u_z}{\partial x} + \frac{\partial u_x}{\partial z}\right) = \frac{1}{2}\gamma_{xz}^{(0)} + \frac{1}{2}z^2\gamma_{xz}^{(2)} \tag{12b}$$

with

$$\begin{Bmatrix} \varepsilon_{xx}^{(0)} \\ \varepsilon_{xx}^{(1)} \\ \varepsilon_{xx}^{(3)} \end{Bmatrix} = \begin{Bmatrix} \dfrac{\partial u}{\partial x} \\ \dfrac{\partial \varphi}{\partial x} \\ -\left(\dfrac{4}{3h^2}\right)\left(\dfrac{\partial \varphi}{\partial x} + \dfrac{\partial^2 w}{\partial x^2}\right) \end{Bmatrix} 7c \tag{13a}$$

$$\begin{Bmatrix} \gamma_{xz}^{(0)} \\ \gamma_{xz}^{(2)} \end{Bmatrix} = \begin{Bmatrix} \dfrac{\partial w}{\partial x} + \varphi \\ -\left(\dfrac{4}{h^2}\right)\left(\dfrac{\partial w}{\partial x} + \varphi\right) \end{Bmatrix} \tag{13b}$$

The resultant normal forces, bending moment, axial force, and shear forces are expressed as, Al-shujairi and Mollamahmutoğlu (2018)

$$\begin{Bmatrix} N \\ M \\ M_h \end{Bmatrix} = \int_A \begin{Bmatrix} 1 \\ z \\ \Phi(z) \end{Bmatrix} \sigma_{xx}^t dA \tag{14a}$$

$$Q_h = \int_A \frac{d\Phi(z)}{dz} \tau_{xz}^t dA \tag{14b}$$

and the higher order stress resultants are given by, Al-shujairi and Mollamahmutoğlu (2018)

$$\begin{Bmatrix} N^h \\ M^h \\ M_h^h \end{Bmatrix} = \int_A \begin{Bmatrix} 1 \\ z \\ \Phi(z) \end{Bmatrix} \sigma_{xx}^h dA \tag{15a}$$

$$Q_h^h = \int_A \frac{d\Phi(z)}{dz} \tau_{xz}^h dA \tag{15b}$$

2.4 The governing equation of motion

The governing dynamic equations of motion can be obtained by applying the Hamilton principle as, Reddy (2017), Al-shujairi and Mollamahmutoğlu (2018)

$$\int_{t1}^{t2} (\delta U_s - \delta T + \delta V) dt = 0. \tag{16}$$

with δU_s, δT, δV are respectively refer to the variations of strain energy, kinetic energy and work done by the external forces which can be expressed as Ebrahimi (2016), Al-shujairi and Mollamahmutoğlu (2018)

$$\delta \int_0^t U_s dt = \int_0^t \int_\Omega \begin{pmatrix} \sigma_{xx}^c \delta\varepsilon_{xx}^c + \tau_{xz}^c \delta\gamma_{xz}^c \\ +\sigma_{xx}^h \nabla\delta\varepsilon_{xx} + \tau_{xz}^h \nabla\delta\gamma_{xz} \end{pmatrix} d\Omega \mathrm{dt} \tag{17a}$$

Using Eqs. (6a)-(6b), Eq. (17a) can be simplified to the following form

$$\begin{aligned} \delta \int_0^t U_s dt = & \int_0^t \int_\Omega (\sigma_{xx}^t \delta\varepsilon_{xx} + \tau_{xz}^t \delta\gamma_{xz}) d\Omega \mathrm{dt} \\ & + \int_0^t \left[\int_A (\sigma_{xx}^h \delta\varepsilon_{xx} + \tau_{xz}^h \delta\gamma_{xz}) dA \right]_0^L dt \end{aligned} \tag{17b}$$

Using Eqs. (14) and (15) and Performing the first variation of the strain energy one can write

$$\begin{aligned} \delta \int_0^t U_s dt = & \int_0^t \int_0^L \left[N \frac{\partial \delta u}{\partial x} - M \frac{\partial^2 \delta w}{\partial x^2} + M_h \left(\frac{\partial^2 \delta w}{\partial x^2} - \frac{\partial \delta \varphi}{\partial x} \right) + Q_h \left(\frac{\partial \delta w}{\partial x} - \delta\varphi \right) \right] d\mathrm{xdt} \\ & + \int_0^t \left[N^h \frac{\partial \delta u}{\partial x} - M^h \frac{\partial^2 \delta w}{\partial x^2} + M_h^h \left(\frac{\partial^2 \delta w}{\partial x^2} - \frac{\partial \delta \varphi}{\partial x} \right) + Q_h^h \left(\frac{\partial \delta w}{\partial x} - \delta\varphi \right) \right]_0^L dt \end{aligned} \tag{17c}$$

The variation of the total kinetic energy can be expressed as

$$\delta \int_0^t T dt = \int_0^t \int_\Omega \rho \left(\frac{\partial u_x}{\partial t} \frac{\partial \delta u_x}{\partial t} + \frac{\partial u_z}{\partial t} \frac{\partial \delta u_z}{\partial t} \right) d\Omega dt \tag{18a}$$

Substituting from Eqs. (11a)-(11c), the variation of the kinetic energy can be expressed as

$$\begin{aligned} \delta \int_0^t T dt = & \int_0^t \int_0^L \left[m_0 \left(\frac{\partial u}{\partial t} \frac{\partial \delta u}{\partial t} + \frac{\partial w}{\partial t} \frac{\partial \delta w}{\partial t} \right) - m_1 \left(\frac{\partial u}{\partial t} \frac{\partial^2 \delta w}{\partial x \partial t} + \frac{\partial^2 w}{\partial x \partial t} \frac{\partial \delta u}{\partial t} \right) + m_3 \left(\frac{\partial^2 w}{\partial x \partial t} \frac{\partial^2 \delta w}{\partial x \partial t} \right) \right. \\ & + m_2 \left(\frac{\partial u}{\partial t} \left(\frac{\partial^2 \delta w}{\partial x \partial t} - \frac{\partial \delta \varphi}{\partial t} \right) + \frac{\partial \delta u}{\partial t} \left(\frac{\partial^2 w}{\partial x \partial t} - \frac{\partial \varphi}{\partial t} \right) \right) \\ & \left. - m_4 \left(\frac{\partial^2 w}{\partial x \partial t} \left(\frac{\partial^2 \delta w}{\partial x \partial t} - \frac{\partial \delta \varphi}{\partial t} \right) + \frac{\partial^2 \delta w}{\partial x \partial t} \left(\frac{\partial^2 w}{\partial x \partial t} - \frac{\partial \varphi}{\partial t} \right) \right) + m_5 \left(\left(\frac{\partial^2 w}{\partial x \partial t} - \frac{\partial \varphi}{\partial t} \right) \left(\frac{\partial^2 \delta w}{\partial x \partial t} - \frac{\partial \delta \varphi}{\partial t} \right) \right) \right] dx dt \end{aligned} \tag{18b}$$

where the mass moments of inertia can be expressed as, Xie *et al*. (2020) and Al-shujairi and Mollamahmutoğlu (2018)

$$(m_0, m_1, m_2, m_3, m_4, m_5) = \int_{-\frac{h}{2}}^{\frac{h}{2}} \rho \times (1, z, \Phi(z), z^2, z\Phi(z), (\Phi(z))^2) dA \tag{18c}$$

The variation of the work done by applied external mechanical and magnetic loads is expressed in the following form

$$\delta V = \int_0^l \left(P_x \left[\frac{\partial \delta u}{\partial x} + \frac{\partial w}{\partial x} \frac{\partial \delta w}{\partial x} \right] + q\delta w + f\delta u \right) dx \tag{19}$$

where P_x is the applied axial buckling load and q and f are respectively the transverse and axial distributed loads per unit length. Applying the Hamilton's principle and evaluating the integral and setting each coefficient of $\delta u, \delta w$ and $\delta\varphi$ to zero, the equations of motion based on the third order higher order shear deformation beam theory are

Substitute Eq. (21c) into Eqs. (20), the following differential equations of motion in terms of displacement field are obtained

$$\begin{aligned}
&\frac{\partial N}{\partial x} + f = m_0 \frac{\partial^2 u}{\partial t^2} + (m_1 - m_2) \frac{\partial^3 w}{\partial x \partial t^2} - m_2 \frac{\partial^2 \varphi}{\partial t^2} \\
&\frac{\partial^2 M}{\partial x^2} - \frac{\partial^2 M_h}{\partial x^2} + \frac{\partial Q_h}{\partial x} - (P_x) \frac{\partial^2 w}{\partial x^2} = m_0 \frac{\partial^2 w}{\partial t^2} + (m_1 - m_2) \frac{\partial^3 u}{\partial x \partial t^2} - (m_5 - 2m_4 + m) \frac{\partial^4 w}{\partial x^2 \partial t^2} + (m_4 - m_5) \frac{\partial^3 \varphi}{\partial x \partial t^2} \\
&Q_h - \frac{\partial M_h}{\partial x} = -m_2 \frac{\partial^2 u}{\partial t^2} + (m_4 - m_5) \frac{\partial^3 w}{\partial x \partial t^2} + m_5 \frac{\partial^2 \varphi}{\partial t^2}
\end{aligned} \tag{20}$$

The stress resultants stresses can be expressed in terms of displacements as

$$\begin{aligned}
&\left(1 - (ea)^2 \frac{\partial^2}{\partial x^2}\right) N = \left(1 - l_m^2 \frac{\partial^2}{\partial x^2}\right) \left(D_0 \frac{\partial u}{\partial x} + (D_2 - D_1) \frac{\partial^2 w}{\partial x^2} - D_2 \frac{\partial \varphi}{\partial x} \right) \\
&\left(1 - (ea)^2 \frac{\partial^2}{\partial x^2}\right) M = \left(1 - l_m^2 \frac{\partial^2}{\partial x^2}\right) \left(D_0 \frac{\partial u}{\partial x} + (D_4 - D_3) \frac{\partial^2 w}{\partial x^2} - D_4 \frac{\partial \varphi}{\partial x} \right) \\
&\left(1 - (ea)^2 \frac{\partial^2}{\partial x^2}\right) Q_h = G_0 \left(1 - l_m^2 \frac{\partial^2}{\partial x^2}\right) \left(\frac{\partial w}{\partial x} - \varphi \right) \\
&\left(1 - (ea)^2 \frac{\partial^2}{\partial x^2}\right) M_h = \left(1 - l_m^2 \frac{\partial^2}{\partial x^2}\right) \left(D_2 \frac{\partial u_0}{\partial x} - (D_5 - D_4) \frac{\partial^2 w}{\partial x^2} - D_5 \frac{\partial \varphi}{\partial x} \right)
\end{aligned} \tag{21a}$$

with

$$\begin{aligned}
&[D_0 \quad D_1 \quad D_2 \quad D_3 \quad D_4 \quad D_5] = \int_A E\left[1 \quad z \quad \Phi(z) \quad z^2 \quad z\Phi(z) \quad (\Phi(z))^2\right] dA \\
&G_0 = \int_A G \left(\frac{d\Phi(z)}{dz} \right)^2 dA
\end{aligned} \tag{21b}$$

Therefore, Eq. (21a) can be expressed in terms of the displacement field as

$$\begin{aligned}
N &= (ea)^2 \left(m_0 \frac{\partial^3 u}{\partial x \partial t^2} + (m_1 - m_2) \frac{\partial^4 w}{\partial x^2 \partial t^2} - m_2 \frac{\partial^3 \varphi}{\partial x \partial t^2} - \frac{\partial f}{\partial x} \right) + \left(1 - l_m^2 \frac{\partial^2}{\partial x^2}\right) \left(D_0 \frac{\partial u}{\partial x} + (D_2 - D_1) \frac{\partial^2 w}{\partial x^2} - D_2 \frac{\partial \varphi}{\partial x} \right) \\
M &= (ea)^2 \left(m_0 \frac{\partial^2 w}{\partial t^2} + m_1 \frac{\partial^3 u}{\partial x \partial t^2} + (m_4 - m_3) \frac{\partial^4 w}{\partial x^2 \partial t^2} - m_4 \frac{\partial^3 \varphi}{\partial x \partial t^2} + (P_x) \frac{\partial^2 w}{\partial x^2} \right) \\
&\quad + \left(1 - l_m^2 \frac{\partial^2}{\partial x^2}\right) \left(D_0 \frac{\partial u_0}{\partial x} + (D_4 - D_3) \frac{\partial^2 w_0}{\partial x^2} - D_4 \frac{\partial \varphi}{\partial x} \right) \\
Q_h &= (ea)^2 \left(-m_2 \frac{\partial^4 u}{\partial x^2 \partial t^2} - (m_5 - m_4) \frac{\partial^5 w}{\partial x^3 \partial t^2} + m_5 \frac{\partial^4 \varphi}{\partial x^2 \partial t^2} \right) \\
&\quad + \left(1 - l_m^2 \frac{\partial^2}{\partial x^2}\right) \left(D_2 \frac{\partial^2 u}{\partial x^2} - (D_5 - D_4) \frac{\partial^3 w}{\partial x^3} + D_5 \frac{\partial^2 \varphi}{\partial x^2} + G_0 \left(\frac{\partial w}{\partial x} - \varphi \right) \right)
\end{aligned} \tag{21c}$$

$$\begin{aligned}
&\left(1-(ea)^2\frac{\partial^2}{\partial x^2}\right)\left(-m_0\frac{\partial^2 u}{\partial t^2}+(m_1-m_2)\frac{\partial^3 w}{\partial x\partial t^2}+m_2\frac{\partial^2\varphi}{\partial t^2}+f\right)\\
&\qquad+\left(1-l_m^2\frac{\partial^2}{\partial x^2}\right)\left(D_0\frac{\partial^2 u}{\partial x^2}+(D_2-D_1)\frac{\partial^3 w}{\partial x^3}-D_2\frac{\partial^2\varphi}{\partial x^2}\right)=0\\
&\left(1-(ea)^2\frac{\partial^2}{\partial x^2}\right)\left(-m_0\frac{\partial^2 w}{\partial t^2}-m_1\frac{\partial^3 u}{\partial x\partial t^2}-(m_4-m_3)\frac{\partial^4 w}{\partial x^2\partial t^2}+m_4\frac{\partial^3\varphi}{\partial x\partial t^2}-(P_x)\frac{\partial^2 w}{\partial x^2}\right)\\
&\qquad+\left(1-l_m^2\frac{\partial^2}{\partial x^2}\right)\left(D_1\frac{\partial^3 u}{\partial x^3}+(D_4-D_3)\frac{\partial^4 w}{\partial x^4}-D_4\frac{\partial^3\varphi}{\partial x^3}\right)=0\\
&\left(1-(ea)^2\frac{\partial^2}{\partial x^2}\right)\left(m_2\frac{\partial^2 u}{\partial t^2}+(m_5-m_4)\frac{\partial^3 w}{\partial x\partial t^2}-m_5\frac{\partial^2\varphi}{\partial t^2}\right)\\
&\qquad+\left(1-l_m^2\frac{\partial^2}{\partial x^2}\right)\left(-D_2\frac{\partial^2 u}{\partial x^2}-(D_5-D_4)\frac{\partial^3 w}{\partial x^3}+D_5\frac{\partial^2\varphi}{\partial x^2}+G_0\left(\frac{\partial w}{\partial x}-\varphi\right)\right)=0
\end{aligned}\tag{22a}$$

Neglecting the nonclassical effects, the governing equations can be written as

$$\begin{aligned}
&\left(-m_0\frac{\partial^2 u}{\partial t^2}+(m_1-m_2)\frac{\partial^3 w}{\partial x\partial t^2}+m_2\frac{\partial^2\varphi}{\partial t^2}+f\right)+\left(D_0\frac{\partial^2 u}{\partial x^2}+(D_2-D_1)\frac{\partial^3 w}{\partial x^3}-D_2\frac{\partial^2\varphi}{\partial x^2}\right)=0\\
&\left(-m_0\frac{\partial^2 w}{\partial t^2}-m_1\frac{\partial^3 u}{\partial x\partial t^2}-(m_4-m_3)\frac{\partial^4 w_0}{\partial x^2\partial t^2}+m_4\frac{\partial^3 C}{\partial x\partial t^2}-(P_x)\frac{\partial^2 w}{\partial x^2}\right)\\
&\quad+\left(D_1\frac{\partial^3 u}{\partial x^3}+(D_4-D_3)\frac{\partial^4 w}{\partial x^4}-D_4\frac{\partial^3\varphi}{\partial x^3}\right)=0\\
&\left(m_2\frac{\partial^2 u}{\partial t^2}+(m_5-m_4)\frac{\partial^3 w}{\partial x\partial t^2}-m_5\frac{\partial^2\varphi}{\partial t^2}\right)+\left(-D_2\frac{\partial^2 u}{\partial x^2}-(D_5-D_4)\frac{\partial^3 w}{\partial x^3}+D_5\frac{\partial^2\varphi}{\partial x^2}+G_0\left(\frac{\partial w}{\partial x}-\varphi\right)\right)=0
\end{aligned}\tag{22b}$$

Moreover, the corresponding boundary conditions at $x = 0$ and $x = L$ as follows

$$\begin{aligned}
&\delta u(N)=0\Rightarrow N=0 \ \text{ Or } \ u=0\\
&\frac{\partial\delta u}{\partial x}(N^h)=0\Rightarrow N^h=0 \ \text{ Or } \ \frac{\partial u}{\partial x}=0\\
&\delta w\left(\frac{\partial M}{\partial x}-\frac{\partial M_h}{\partial x}+Q_h+(P_x)\frac{\partial w}{\partial x}\right)=0\Rightarrow\frac{\partial M}{\partial x}-\frac{\partial M_h}{\partial x}+Q_h+(P_x)\frac{\partial w_0}{\partial x}=0 \text{ or } w=0\\
&\frac{\partial\delta w}{\partial x}(M)=0\Rightarrow\frac{\partial w}{\partial x}=0 \ \ or \ \ M=0\\
&\frac{\partial^2\delta w}{\partial x^2}(M^h)=0\Rightarrow\frac{\partial^2 w}{\partial x^2}=0 \ \ or \ \ M^h=0\\
&\delta\left(\frac{\partial^2 w}{\partial x^2}-\frac{\partial\varphi}{\partial x}\right)(M^h)=0\Rightarrow\frac{\partial^2 w}{\partial x^2}-\frac{\partial\varphi}{\partial x}=0 \ \ or \ \ M^h=0\\
&\delta\left(\frac{\partial w}{\partial x}-\varphi\right)(Q^h+M_h)=0\Rightarrow\frac{\partial w}{\partial x}-\varphi=0 \ \ or \ \ Q^h+M_h=0
\end{aligned}\tag{23}$$

Considering perforated beam with rectangular cross section, with width w_b and depth h, the equivalent inertia and stiffnesses can be expressed as

$$[m_0 \quad m_1 \quad m_2 \quad m_3 \quad m_4 \quad m_5]=\left[(\rho A)_{eq} \quad 0 \quad 0 \quad (\rho I)_{eq} \quad \frac{4}{5}(\rho I)_{eq} \quad \frac{68}{105}(\rho I)_{eq}\right]\tag{24a}$$

$$\begin{aligned}
&[D_0 \quad D_1 \quad D_2 \quad D_3 \quad D_4 \quad D_5]=\left[(EA)_{eq} \quad 0 \quad 0 \quad (EI)_{eq} \quad \frac{4}{5}(EI)_{eq} \quad \frac{68}{105}(EI)_{eq}\right]\\
&G_0=\frac{8}{15}(GA)_{eq}
\end{aligned}\tag{24b}$$

3. Analytical solution procedure

For the simply supported boundary conditions, Navier's approach will be used to define the vibration frequencies and displacements. Assuming the vibration solution is periodic in time, the displacements are in the form

$$\begin{aligned} u(x,t) &= \sum_n U_n \cos\beta x\, e^{i\omega_n t} \\ w(x,t) &= \sum_n W_n \sin\beta x\, e^{i\omega_n t} \\ \varphi(x,t) &= \sum_n \Phi_n \cos\beta x\, e^{i\omega_n t}, \quad \beta = \left(\frac{n\pi}{L}\right) \end{aligned} \tag{25}$$

where $i = \sqrt{-1}$, and ω_n is the natural vibration frequencies. For any W_n and Φ_n, the series solution (25) satisfies the classical and non-classical boundary conditions in (23). Neglecting the external and buckling forces and substituting Eq. (25) into Eq. (22a) the following eigen value equation is derived.

$$\sum_{n=1}^{N}\left[[\boldsymbol{K}] - \omega_n^2[\boldsymbol{M}]\right]\begin{Bmatrix} U_n \\ W_n \\ \Phi_n \end{Bmatrix} = \begin{Bmatrix} 0 \\ 0 \\ 0 \end{Bmatrix} \tag{26}$$

Here, $\mathbf{d} = \{U_n \quad W_n \quad \Phi_n\}^{\boldsymbol{T}}$ are the unknowns to be determined, **K** and **M** are stiffness and mass matrices, respectively. Considering the external load, Eq. (25) can be written as

$$\sum_{n=1}^{N}\left[[\boldsymbol{K}] - \omega_n^2[\boldsymbol{M}]\right]\begin{Bmatrix} U_n \\ W_n \\ \Phi_n \end{Bmatrix} = \begin{Bmatrix} 0 \\ -q \\ 0 \end{Bmatrix} \tag{27a}$$

These matrices are described as follows

$$\mathbf{K} = C_1\begin{bmatrix} D_0\beta^2 & (D_2 - D_1)\beta^3 & D_2\beta^2 \\ -D_1\beta^3 & (D_3 - D_4)\beta^4 & D_4\beta^3 \\ -D_2\beta^2 & -\big((D_5 - D_4)(\beta)^3 + G_0\beta\big) & (D_5(\beta)^2 + G_0) \end{bmatrix} \tag{27b}$$

$$\mathbf{M} = c_2\begin{bmatrix} m_0 & -(m_1 - m_2)\beta & -m_2 \\ -m_1\beta & (m_0 - (m_4 - m_3)\beta^2) & m_4\beta \\ -m_2 & -(m_5 - m_4)\beta & m_5 \end{bmatrix}, \tag{27c}$$

$$c_2 = 1 + (ea)^2\beta^2, \qquad c_1 = 1 + l_m^2\beta^2 \tag{27d}$$

For the forced vibration response of the Timoshenko nanobeamcs could be obtained by solving Eq. (27a) as. Where **q** is the external force vector and it can be defined according to the type of the transverse load $q(x)$ as given below, Reddy (2007)

$$\mathbf{q} = \begin{Bmatrix} 0 \\ Q_n c_2 \\ 0 \end{Bmatrix}. \tag{28}$$

The external load can be expanded in Fourier series and the term Q_n is defined as follows

$$q(x) = \sum_n Q_n \sin\frac{n\pi x}{L} \tag{29a}$$

$$Q_n = \frac{2}{L}\int_0^L q(x)\sin\frac{n\pi x}{L}dx \tag{29b}$$

For point load at x_p, the external load is defined as $q(x) = q_0\delta(x - x_p)$ and Q_n is derived as

$$\begin{aligned} &Q_n = \frac{2F}{L}\sin\left(\frac{n\pi}{L}\right)x_p, && n = 1,2,3,\ldots \\ &x_p = \frac{L}{2};\ \xrightarrow{yields} Q_n = \frac{2F}{L}\sin\frac{n\pi}{2}, && n = 1,2,3,\ldots \end{aligned} \tag{29c}$$

For uniform load

$$q(x) = q_0, \quad Q_n = \frac{4q_0}{n\pi}, \quad n = 1,3,5,\ldots \tag{29d}$$

For moving point load at $x_p = vt$, the external load is defined as $q(x,t) = F\delta(x - vt)$ and Q_n is derived as

$$Q_n = \frac{2F}{L}\sin\frac{n\pi}{L}vt, \quad n = 1,2,3,\ldots \tag{29e}$$

4. Verification of the developed model

To check the accuracy of the proposed nonclassical procedure to investigate the dynamic behaviour of perforated beam structures, consider a fully filled (α = 1) simply supported beam having the following characteristics: the beam length, L = 10 nm, the Poisson's ratio, ν = 0.3 while the nanobeam material characteristics are taken as reported in Salvetat *et al*. (1999). The individual as well as the combined effects of nonlocal and material length scale parameters are verified and compared. The nondimensional frequency parameter, λ_i can be defined as

$$\lambda_i = \omega_i L^2\sqrt{\rho A/EI} \tag{30}$$

4.1 Verification of nonlocal effect

To check the accuracy of the proposed procedure to investigate the nonclassical nonlocal dynamic behaviour of nanobeam, the proposed model is applied to detect the resonant frequencies of the lowest three vibration modes at different values of the nonlocal parameter for different beam aspect ratio, as illustrated in Tables 1 and 2. It may be noticed that an excellent agreement is found between the obtained results and the corresponding results reported by Thai (2012) and Thai and Vo (2012).

Table 1 Comparison between the different results for the fundamental frequency parameter λ_1 at different values of the nonlocal parameter and beam aspect ratio

L/h	$(e_0a)^2$	TBT (Thai 2012)	TBT (Thai and Vo 2012)	TBT present
5	0	9.2740	9.2752	9.2742
	1	8.8477	8.8488	8.8474
	2	8.4752	8.4763	8.4753
	3	8.1461	8.1472	8.1464
	4	7.8526	7.8536	7.8528
10	0	9.7075	9.7077	9.7076
	1	9.2612	9.2614	9.2613
	2	8.8713	8.8715	8.8714
	3	8.5269	8.5271	8.5267
	4	8.2196	8.2198	8.2194
20	0	9.8281	9.8282	9.8282
	1	9.3763	9.3764	9.3762
	2	8.9816	8.9816	8.9815
	3	8.6328	8.6329	8.6329
	4	8.3218	8.3218	8.3214
100	0	9.8679	9.8679	9.8678
	1	9.4143	9.4143	9.4142
	2	9.0180	9.0180	9.0183
	3	8.6678	8.6678	8.6677
	4	8.3555	8.3555	8.3556

Table 2 Comparison between the different results for the 2nd and 3rd frequency parameters λ_2 and λ_3 for different values of the nonlocal parameter at different aspect ratio

L/h	$(e_0a)^2$ nm^2	λ_2		λ_3	
		TBT (Thai and Vo 2012)	TBT Present	TBT (Thai and Vo 2012)	TBT Present
5	0	32.1948	32.1661	61.6192	61.4594
	1	27.2604	27.2353	44.8420	44.7842
	2	24.0664	24.0459	36.9798	36.8944
	3	21.7833	21.7746	32.1878	32.1535
	4	20.0470	20.0390	28.8778	28.8543
10	0	37.1009	37.0983	78.1855	78.1848
	1	31.4146	31.4147	56.8977	56.8953
	2	27.7339	27.7338	46.9219	46.9234
	3	25.1029	25.0996	40.8415	40.8454
	4	23.1019	23.0998	36.6416	36.6472
20	0	38.8308	38.8298	85.6671	85.6673
	1	32.8793	32.8780	62.3422	62.3435
	2	29.0270	29.0269	51.4118	51.4117
	3	26.2733	26.2732	44.7496	44.7499
	4	24.1790	24.1789	40.1478	40.1474
100	0	39.4517	39.4518	88.6915	88.6918
	1	33.4051	33.4052	64.5432	64.5436
	2	29.4912	29.4913	53.2269	53.2265
	3	26.6934	26.6935	46.3295	46.3292
	4	24.5657	24.5658	41.5653	41.5652

Table 3 Comparison between the different results for the frequency parameters for the 1st lowest vibration modes at different values of the microstructure length scale parameter at different values of beam aspect ratio, L/h

L/h	$(l\ nm)$	λ_1		λ_2		λ_3	
		Present	Esen (2020)	Present	Esen (2020)	Present	Esen (2020)
5	0	9.2766	9.2764	32.2621	32.2627	62.1205	62.1201
	0.2h	10.0158	10.0157	34.3264	34.3260	65.2627	65.2623
	0.4h	11.8534	11.8537	39.0495	39.0497	71.9440	71.9444
	0.6h	14.1403	14.1401	44.1238	44.1234	78.3113	78.3111
	0.8h	16.4376	16.4379	48.3779	48.3777	83.0117	83.0111
10	0	9.7075	9.7079	37.1318	37.1319	78.5014	78.5015
	0.2h	10.5434	10.5432	40.1056	40.1058	84.2085	84.2087
	0.4h	12.6872	12.6875	47.4843	47.4840	97.8018	97.8017
	0.6h	15.5322	15.5326	56.7171	56.7174	113.7053	113.7056
	0.8h	18.6551	18.6555	66.0143	66.0146	128.3152	128.3157
20	0	9.8295	9.8291	38.8545	38.8542	85.8491	85.8494
	0.2h	10.6927	10.6921	42.1986	42.1988	93.0193	93.0196
	0.4h	12.9316	12.9319	50.8102	50.8100	111.2637	111.2634
	0.6h	15.9594	15.9593	62.2554	62.2551	134.9304	134.9307
	0.8h	19.3756	19.3752	74.7848	74.7847	159.7735	159.7739

Table 4 Comparison between the different results for the frequency parameters for the 1st lowest vibration modes at different values of nonlocal parameter at different values of beam aspect ratio, L/h

L/h	$(e_0a)^2 = l^2(nm^2)$	λ_1		λ_2		λ_3	
		Present	Esen (2020)	Present	Esen (2020)	Present	Esen (2020)
25	0	9.7885	9.7887	38.2483	38.2481	83.0631	83.0633
	10^{-18}	9.6006	9.6002	35.6154	35.6153	72.0786	72.0789
	2×10^{-18}	9.3575	9.3571	32.7666	32.7664	62.4638	62.4637
	3×10^{-18}	9.1303	9.1307	30.4994	30.4992	55.8704	55.8707
	4×10^{-18}	8.9199	8.9198	28.6436	28.6439	50.9999	50.9998
50	0	9.8505	9.8507	39.1834	39.1831	87.3833	87.3835
	10^{-18}	9.5072	9.5073	34.5186	34.5182	68.4531	68.4533
	2×10^{-18}	9.1733	9.1734	30.9727	30.9724	57.5087	57.5084
	3×10^{-18}	8.8724	8.8721	28.3319	28.3318	50.5444	50.5449
	4×10^{-18}	8.5988	8.5986	26.2685	26.2681	45.6197	45.6199
100	0	9.8644	9.8649	39.4052	39.4057	88.4722	88.4726
	10^{-18}	9.4565	9.4569	33.9443	33.9445	66.6048	66.6044
	2×10^{-18}	9.0783	9.0787	30.1125	30.1122	55.2293	55.2291
	3×10^{-18}	8.7426	8.7424	27.3386	27.3387	48.2053	48.2059
	4×10^{-18}	8.4409	8.4407	25.2129	25.2126	43.3213	43.3217

4.2 Verification of microstructure effect

Neglecting the nonlocal effect, comparison between the obtained nondimensional frequency parameters with the material length scale parameter at different beam aspect ratio obtained by the developed model and those obtained by Esen (2020), shows that the two results are very close validating the developed model, as illustrated in Table 3. From this table, it can be concluded that, the natural frequencies are influenced by slenderness ratio. As the slenderness ratio increased the natural frequencies are increased.

4.3 Verification of the coupled effect of nonlocal and microstructure

Considering the combined effect of nonlocal and material length scale parameter, comparison between the obtained nondimensional frequency parameters for different values of equal nonlocal and material length scale parameter for different beam aspect ratio and the corresponding results obtained by Esen (2020) are depicted in Table 4. It is seen that good agreement is found.

4.4 Verification of classical forced vibration behavior under moving load

To check the accuracy of the developed methodology to study and analyze the classical forced vibration behavior under moving load, consider a simply supported beam with the following characteristics: length, L = 1 m, elasticity modulus, E = 207 GPa, shear modulus, G = 77.6 GPa, shear correction facto, k_s = 0.9, and mass density, ρ = 7700 kg/m^3. The cross-sectional area of the beam, A is computed from the radius of gyration r_0 defined by a nondimensional parameter, $= \frac{\pi r_0}{L}$. The nondimensional speed parameter of the moving load is given, in terms of the moving load velocity, v and the critical velocity, v_{cr} as $\beta = v/v_{cr}$, where v_{cr} for a supported beam is given by $vcr = \frac{\pi}{L}\sqrt{\frac{EI}{\rho A}}$. This problem has been previously studied numerically by Lou *et al.* (2007) and analytically by Kim *et al.* (2017). The normalized deflection, $W_{rel} = \frac{w_{max}\left(\frac{L}{2}, t\right)}{w_{stat}}$ versus the normalized coordinate, $\frac{x_p(t)}{L}$ is presented in Fig. 2. It may be noticed that good agreement is found verifying the developed methodology.

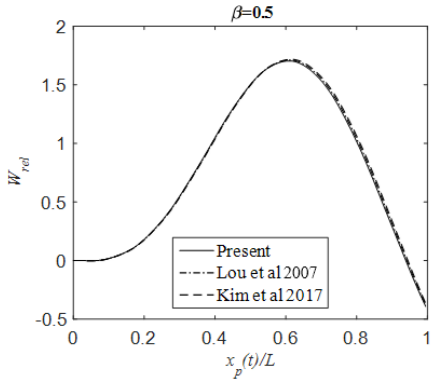

Fig. 2 The dynamic magnification factor profile with the nondimensional coordinate for speed parameter β = 0.5 for classical analysis

5. Numerical results

Within this section, the applicability of the developed methodology is demonstrated. Consider the regularly squared perforated higher order Reddy nanobeam presented in section 4. The developed methodology is applied to investigate both free and forced vibration behavior under moving mass.

5.1 Free vibration of perforated nanobeam

Neglecting the nonclassical effects, the dependency of the classical nondimensional frequency parameters of the lowest three vibration modes on filling ratio at different values of beam aspect ratio is illustrated in Table 5. It is seen that the nondimensional frequency parameters are increased with increasing beam aspect ratio and/or perforation filling ratio due to increasing the overall beam stiffness. Additionally, the absolute relative percentage difference, $\%\Delta\lambda_i = \left|\frac{(\lambda_i)_{\alpha=0.3}-(\lambda_i)_{\alpha=1}}{(\lambda_i)_{\alpha=1}}\right| \times 100$ significantly affected by beam aspect ratio; it is decreased with increasing beam aspect ratio especially at higher vibration modes.; at the 1st vibration mode this percentage reaches 12.27% for L/h = 10 and 11.6% for L/h = 30. While at the 3rd vibration mode it reaches about 9% for L/h = 10 and 2.35% for L/h = 30.

Neglecting the nonlocal effect, incorporating the nonclassical macrostructure effect significantly affects the free vibration behavior of higher order perforated nanobeams. Variations of the nondimensional frequency parameters versus the normalized microstructure material parameter, (l/h) at different perforation filling ratio is illustrated in Table 6. It may be noticed that introduction of the microstructure effect results in material stiffening thus larger values of the nondimensional frequency parameters are detected with increasing the normalized microstructure length scale parameter. This effect is more significant at

Table 5 Dependency of the first three frequency parameters on filling ratio for classical perforated nanobeam, $l = e_0 a = 0$, and $N = 6$

	λ_1		λ_2		λ_3	
α	L/h = 10	L/h = 30	L/h = 10	L/h = 30	L/h = 10	L/h = 30
0.2	6.7580543	6.9034729	28.029116	30.690905	67.181511	82.096001
0.4	7.0485620	7.1099191	28.610832	29.644604	65.994812	71.617821
0.6	7.3762460	7.4226222	29.819607	30.595516	68.311684	72.525543
0.8	7.5986476	7.6395473	30.671839	31.354448	70.082932	73.794670
1	7.7032118	7.8090115	31.533752	33.372730	73.818504	84.072449

Table 6 Dependency of the first three frequency parameters on the normalized microstructure length scale parameter, l/h, for nonclassical perforated nanobeam, $e_0 a = 0$ and $N = 6$

	λ_1			λ_2			λ_3		
	Filling Ratio, α								
l/h	0.35	0.65	1	0.35	0.65	1	0.35	0.65	1
0	6.9642	7.4453	7.7032	28.3298	30.0835	31.5338	65.5900	68.8572	73.8185
0.1	6.96765	7.44880	7.70701	28.3857	30.1428	31.5960	65.8807	69.1623	74.1457
0.3	6.99507	7.47824	7.73735	28.8287	30.6132	32.0891	68.1614	71.5566	76.7124
0.5	7.04959	7.53655	7.79767	29.6945	31.5331	33.0533	72.5079	76.1196	81.6042
0.7	7.13061	7.62310	7.88727	30.9489	32.8646	34.4490	78.5781	82.4922	88.4360

Table 7 Variation of the relative percentage difference, $\%\Delta\lambda_i$ with the microstructure length scale parameter, l at different values of the perforation filling ratio α, for $e_0 a = 0$, $N = 6$ and L/h = 10

	$\%\Delta\lambda_1$			$\%\Delta\lambda_2$			$\%\Delta\lambda_3$		
	Filling Ratio, α								
l/h	0.35	0.65	1	0.35	0.65	1	0.35	0.65	1
0.1	9.549	3.303	0.049	9.983	4.411	0.197	10.753	6.308	0.443
0.3	9.193	2.920	0.443	8.578	2.919	1.761	7.664	3.064	3.920
0.5	8.485	2.163	1.226	5.833	0.002	4.819	1.775	3.117	10.547
0.7	7.433	1.040	2.390	1.855	4.220	9.245	6.448	11.750	19.802

higher values of beam filling ratio. Moreover, keeping constant value of the normalized microstructure length scale parameter, increasing the perforation filling ratio also increases the perforated nanobeam stiffness, which results in larger values of the nondimensional frequency parameters for all vibration modes.

The absolute relative percentage difference, $\%\Delta\lambda_i = \left|\frac{(\lambda_i)_{NCL}-(\lambda_i)_{CL,\alpha=1}}{(\lambda_i)_{CL,\alpha=1}}\right| \times 100$ significantly influenced by the normalized microstructure parameter, *l*/*h*. As illustrated in Table 7, this percentage difference decreases with increasing *l*/*h* and perforation filling ratio, α especially for smaller values of α and lower vibration modes. □n the other hand for fully filled solid beam; α = 1 this percentage difference increases with increasing *l*/*h*. For perforation filling ratio 0.5 < α < 1.0, %Δλ decreases as 0 < *l*/*h* < 0.5 and then increases for *l*/*h* > 0.5.

Neglecting the microstructure effect, introduction of the nonclassical nonlocal effect greatly affects the nondimensional frequency parameters, as depicted in Table 8. The dimensionless frequency parameters are investigated at different nonlocal parameters, $(e_0a)^2$ 0, 1, 2, 3, and 5; Li *et al*. (2019). In contrary the microstructure effect, incorporation of the nonlocal effect, results in material softening and lead to reduction of the overall system stiffness. The dependency of the nondimensional frequency parameters on the nonlocal parameter at different filling ratio is depicted in Table 8. It is observed that the nondimensional frequency parameters decreases with increasing the nonlocal parameter for all values of filling ratio at all vibration modes. This effect is more significant at higher vibration modes.

The absolute relative percentage difference, $\%\Delta\lambda_i = \left|\frac{(\lambda_i)_{NCL}-(\lambda_i)_{CL,\alpha=1}}{(\lambda_i)_{CL,\alpha=1}}\right| \times 100$significantly affected by the nonlocality parameter; it is increased with increasing the

Table 8 Dependency of the first three frequency parameters, for nonclassical perorated nanobeam, on the nonlocality parameter for *l* = 0, *L*/*h* = 10 and *N* = 6

	λ_1			λ_2			λ_3		
	Filling Ratio, α								
$(e_0a)^2$	0.35	0.65	1	0.35	0.65	1	0.35	0.65	1
0	6.9642	7.4453	7.7032	28.3298	30.0835	31.5338	65.5900	68.8572	73.8185
1	6.8437	7.31638	7.5699	26.5086	28.1495	29.5066	57.0937	59.9376	64.2562
2	6.5165	6.9666	7.2080	22.6205	24.0208	25.1788	43.4466	45.6108	48.8971
3	6.0621	6.4808	6.7054	18.7656	19.9272	20.8879	33.307	34.9661	37.4854
5	5.0680	5.4181	5.6058	13.2768	14.0987	14.7783	21.8702	22.9596	24.6139

Table 9 Variation of the relative percentage difference, $\%\Delta\lambda_i$ with the nonlocality parameter, e_0a at different values of the perforation filling ratio α, for $l = 0$, *N* = 6 and *L*/*h* = 10

	λ_1			λ_2			λ_3		
	Filling Ratio, α								
$(e_0a)^2$	0.35	0.65	1	0.35	0.65	1	0.35	0.65	1
1	11.158	5.022	1.730	15.936	10.732	6.429	22.657	18.804	12.954
2	15.405	9.562	6.428	28.266	23.825	20.153	41.144	38.212	33.760
3	21.304	15.869	12.953	40.491	36.807	33.760	54.880	52.632	49.220
5	34.209	29.664	27.228	57.897	55.290	53.135	70.373	68.897	66.656

Table 10 Dependency of the first three frequency parameters on the nonlocality parameter for nonclassical perorated nanobeam, at different values of the normalized microstructure length scale parameter, l/h for *L*/*h* = 10, α = 0.6 and *N* = 6

	λ_1			λ_2			λ_3		
	l/*h*								
$(e_0a)^2$	0.2	0.4	0.6	0.2	0.4	0.6	0.2	0.4	0.6
0	7.3907	7.4342	7.5060	30.0541	30.7470	31.8683	69.5147	73.0048	78.4775
1	7.2628	7.3056	7.3762	28.1221	28.7704	29.8196	60.5099	63.5479	68.3117
2	6.9156	6.9563	7.0235	23.9974	24.5506	25.4459	46.0463	48.3581	51.9832
3	6.4333	6.4712	6.5337	19.9078	20.3667	21.1094	35.2999	37.0722	39.8513
5	5.3784	5.4101	5.4624	14.0849	14.4096	14.9350	23.1788	24.3425	26.1673

Table 11 Variation of the relative percentage difference, $\%\Delta\lambda_i$ with the nonlocality parameter, e_0a at different values of the normalized microstructure length scale parameter, l/h for $N = 6$, $\alpha = 0.6$ and $L/h = 10$

	$\%\Delta\lambda_1$			$\%\Delta\lambda_2$			$\%\Delta\lambda_3$		
	l/h								
$(e_0a)^2$	0.2	0.4	0.6	0.2	0.4	0.6	0.2	0.4	0.6
0	4.057	3.492	2.560	4.692	2.495	1.061	5.830	1.102	6.311
1	5.717	5.161	4.245	10.819	8.763	5.436	18.029	13.913	7.460
2	10.224	9.696	8.824	23.899	22.145	19.306	37.622	34.491	29.580
3	16.485	15.993	15.182	36.868	35.413	33.058	52.180	49.779	46.014
5	30.180	29.768	29.089	55.334	54.304	52.638	68.600	67.024	64.552

nonlocal parameter and decreases with increasing filling ratio. More significant difference is observed at higher vibration modes especially at smaller values of α, see Table 9. Incorporating the coupled nonlocal and microstructure effects significantly affects the nondimensional frequency parameters. Variations of the nondimensional frequency parameters with the nonlocal effect at different normalized microstructure parameter are illustrated in Table 10.

It is observed that keeping constant value of the nonlocal parameter, nondimensional frequency parameters increase with increasing the normalized microstructure length scale parameter, l/h due its stiffening effect. On the other hand, due to its softening effect, keeping constant value of the normalized length scale parameter, l/h, smaller values of the nondimensional frequency parameters are detected by increasing the nonlocal parameter. This effect is more significant at higher values of perforation filling ratio at higher vibration modes.

Dependency of the absolute relative percentage difference, $\%\Delta\lambda_i = \left|\frac{(\lambda_i)_{NCL}-(\lambda_i)_{CL,\alpha=1}}{(\lambda_i)_{CL,\alpha=1}}\right| \times 100$ on the nonlocal parameter at different normalized length scale parameters is illustrated in Table 11. It is observed that, keeping the nonlocal parameter constant, increasing the nondimensional microstructure parameter leads to decrease while it is increased with increasing the nonlocal parameter for all vibration modes.

5.2 Forced vibration of perforated Reddy nanobeam under moving load

Within this section, the forced vibration time response of perforated higher order Reddy nanobeam subjected to moving mass/ load is investigated. The dimensionless velocity parameter, $\beta = \frac{v}{v_{cr}}$ with v_{cr} is the critical velocity $v_{cr} = \frac{\omega_{1L}}{\pi}$. The dynamic magnification factor, W_{rel} is defined as the ratio between the maximum dynamic deflection at the perforated nanobeam midspan and the maximum static deflection due to central load, $W_{rel} = \frac{w_{max}\left(\frac{L}{2},\ t\right)}{w_{stat}}$.

Dependency of the dynamic magnification factor, W_{rel} on the moving load dimensionless velocity parameter, β at different material length scale parameter, l is shown in Fig. 3. It is observed that, neglecting the nonlocal effect, the maximum magnification factor decreases with increasing the material length scale parameter due to increasing the overall system stiffness. On the other hand, oscillating magnification factor profiles are detected for $0 < \beta < 0.25$ due to the dynamic effect associated with the moving load. Additionally, the maximum values of the dynamic magnification factor are observed at $0.5 < \beta < 1$ for all values of the material length scale parameter.

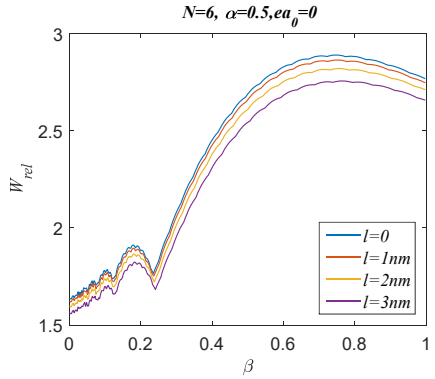

Fig. 3 Variation of the dynamic magnification factor, W_{rel} with the nondimensional velocity parameter, at different values of material length scale parameters for perforated Reddy nanobeam

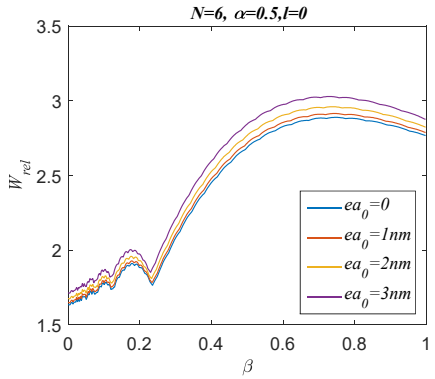

Fig. 4 Variation of the dynamic magnification factor, W_{rel} with the nondimensional velocity parameter, at different values of nonlocal parameter for perforated Reddy nanobeam

Introduction of the nonlocal effect in the absence of the microstructure size effect significantly affects the forced vibration time response under moving load. As illustrated in Fig. 4, it is seen that incorporation of the nonlocal parameter results in material softening which increases the material flexibility thus larger values of the dynamic magnification factor are observed compared with the corresponding classical case. Additionally, oscillating zone of the dynamic magnification factor profile occurs at smaller values of the moving load speed parameter, β ($0 < \beta < 0.25$) for both classical and nonclassical cases.

The dimensionless speed parameter significantly affects the force vibration time response under moving load. The dynamic magnification factor can be obtained by two different ways. The first way is to normalize the dynamic midspan deflection to the corresponding static displacement due to the central load on the perforated beam (normalized by itself). The second normalization way is to normalize the maximum dynamic midspan deflection of the perforated beam to the central static deflection of the corresponding solid beam (normalized by solid beam). The dynamic magnification factor profile throughout the normalized coordinate at different perforation ratio normalized by itself

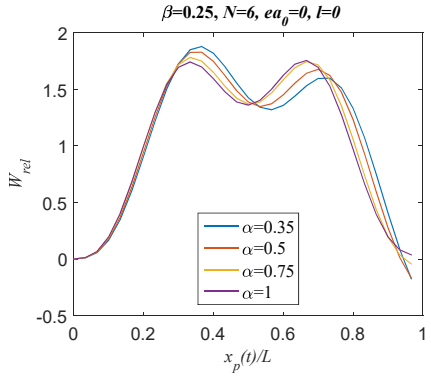

Fig. 5 Variation of the dynamic magnification factor versus the normalized coordinate at different values of α for speed parameter $\beta = 0.25$, material size parameter $l = 0$; nonlocal parameter $e_0a = 0$, and $N = 6$, normalized by itself

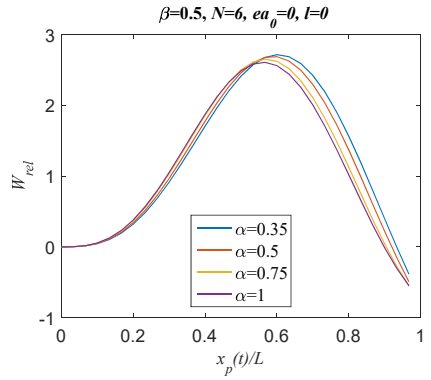

Fig. 6 Variation of the dynamic magnification factor versus the normalized coordinate at different values of α for $\beta = 0.5$, $l = 0$; $e_0a = 0$, and $N = 6$, normalized by itself

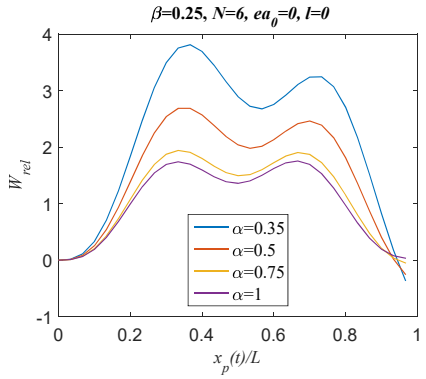

Fig. 7 Variation of the dynamic magnification factor profile with the normalized coordinate for $\beta = 0.25$, for classical analysis, normalized by solid beam

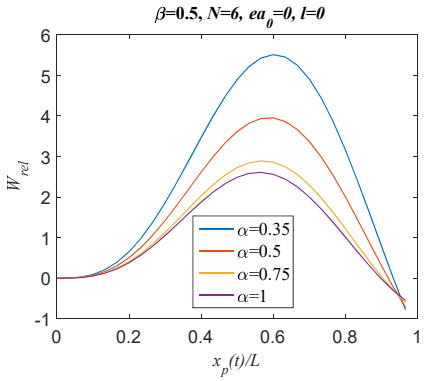

Fig. 8 Variation of the dynamic magnification factor profile with the normalized coordinate for $\beta = 0.5$, for classical analysis, normalized by solid beam

for $\beta = 0.25$ and 0.5 for classical analysis are respectively shown in Figs. 5 and 6. It is observed that dynamic magnification factor oscillating profiles are detected at $\beta = 0.25$ due to the dynamic effect these oscillations disappeared at $\beta = 0.5$. Moreover, slight decrease in the dynamic magnification factor is observed with increasing α.

The dynamic magnification factor profile throughout the nondimensional coordinate, $xp(t)/L$ normalized to the corresponding solid beam at different α for classical analysis for $\beta = 0.25$ and 0.5 are respectively shown in Figs. 7 and 8. Compared to normalized by itself, it is noticed that significant decrease in the maximum magnification factor is observed with increasing α.

Neglecting the nonclassical nonlocal effect, introduction of the microstructure effect results in material stiffening this produces smaller values of the dynamic magnification factor Moreover, wavy dynamic magnification factor profiles are observed at smaller values of β ($\beta = 0.25$) while almost quasistatic profiles are observed at higher values of β ($\beta = 0.5$); see Figs. 9 and 10.

Considering the nonlocal effect in the absence of the microstructure effect causes material softening. This increase the material flexibility thus larger values of the dynamic magnification factors are obtained as e_0a increases. Also oscillating dynamic magnification factor profiles are predicted at $\beta = 0.25$ due to the dynamic effect while

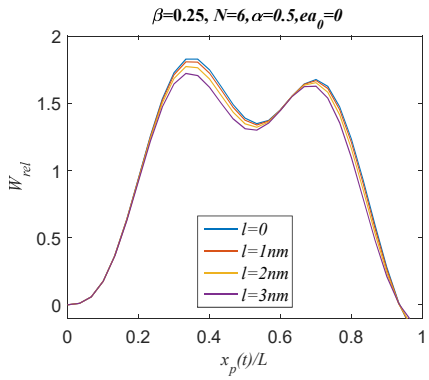

Fig. 9 Variation of the dynamic magnification factor profile with the normalized coordinate for speed parameter $\beta = 0.25$ at different values of microstructure parameter

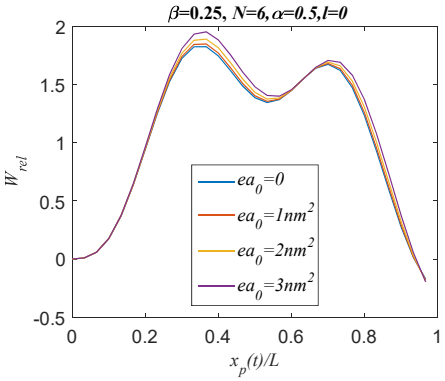

Fig. 11 Variation of the dynamic magnification factor profile with the normalized coordinate for speed parameter $\beta = 0.25$ at different values of nonlocal parameter

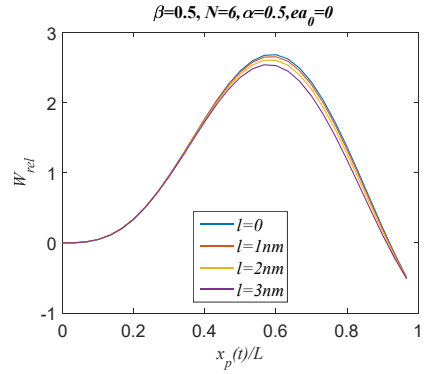

Fig. 10 Variation of the dynamic magnification factor profile with the normalized coordinate for speed parameter $\beta = 0.5$ at different values of microstructure parameter

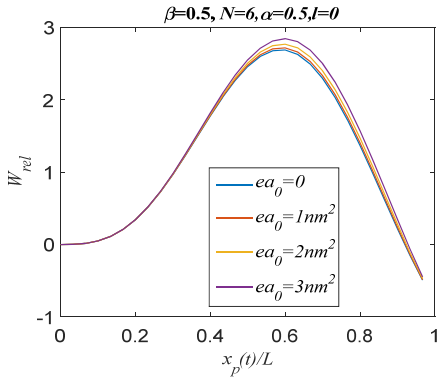

Fig. 12 Variation of the dynamic magnification factor profile with the normalized coordinate for speed parameter $\beta = 0.5$ at different values of nonlocal parameter

smooth profiles are observed at $\beta = 0.5$; see Figs. 11 and 12.

6. Conclusions

In the framework of nonclassical continuum mechanics, a size dependent model based on the nonlocal strain gradient theory is developed to study and analyze the dynamic behaviour of perforated higher order Reddy nanobeams under moving load. Closed forms for the equivalent geometrical and material characteristics of regularly squared perforated beam are presented. Based on the virtual displacement principle, the dynamic equations of motions are derived. An analytical methodology is developed to obtain both free and forced vibration response under moving load. The following concluding remarks are summarized based on the obtained numerical:

- Perforation filling ratio significantly affects the dynamic behaviour of perforated nanobeam structures; increasing the filling ratio results in material stiffening. So, both free and forced vibration behaviour under moving load could be controlled by selecting a suitable value of perforation filling ratio.
- Incorporation of the nonclassical microstructure effect leads to material stiffening which decreases system flexibility. Thus, the nondimensional frequency parameters increase with increasing the microstructure length scale parameter while the dynamic magnification factor decreases.
- Introduction of the nonclassical nonlocal effect results in material softening effect. This increases the material flexibility which produces smaller values of the nondimensional frequency parameters and larger values of the dynamic magnification factor.
- The relative percentage difference between the nonclassical and the corresponding classical nondimensional frequency parameter is significantly affected by both microstructure length scale and nonlocal parameter. This percentage difference increases with increasing the nonlocal parameter for all values of the perforation filling ratio while the effect of the microstructure length scale parameter is dependent on the perforation filling ratio.
- The nondimensional speed parameter significantly affects the stability of the forced vibration time response; □scillating dynamic magnification factor

profiles are detected at smaller values of β these oscillations disappear when selecting larger values of β.

References

Abdelrahman, A.A. and Eltaher, M.A. (2020), "□n bending and buckling responses of perforated nanobeams including surface energy for different beams theories", *Eng. Comput*., 1-27. https://doi.org/10.1007/s00366-020-01211-8

Abdelrahman, A.A., Eltaher, M.A., Kabeel, A.M., Abdraboh, A.M. and Hendy, A.A. (2019), "Free and forced analysis of perforated beams", *Steel Compos. Struct*., *Int. J*., **31**(5), 489-502. https://doi.org/10.12989/scs.2019.31.5.489

Abdelrahman, A.A., Mohamed, N.A. and Eltaher, M.A. (2020a), "Static bending of perforated nanobeams including surface energy and microstructure effects", *Eng. Comput*., 1-21. https://doi.org/10.1007/s40430-019-1996-0

Abdelrahman, A.A., Abd-El-Mottaleb, H.E. and Eltaher, M.A. (2020b), "□n bending analysis of perforated microbeams including the microstructure effects", *Struct. Eng. Mech*., *Int. J*., **76**(6), 765-779. http://dx.doi.org/10.12989/sem.2020.76.6.765

Abdelrahman, A.A., Esen, I., Özarpa, C. and Eltaher, M.A. (2021), "Dynamics of perforated nanobeams subject to moving mass using the nonlocal strain gradient theory", *Appl. Mathe. Modell*., **96**, 215-235. https://doi.org/10.1016/j.apm.2021.03.008

Abo-Bakr, R.M., Eltaher, M.A. and Attia, M.A. (2020a), "Pull-in and freestanding instability of actuated functionally graded nanobeams including surface and stiffening effects", *Eng. Comput*., 1-22. https://doi.org/10.1007/s00366-020-01146-0

Abo-Bakr, H.M., Abo-Bakr, R.M., Mohamed, S.A. and Eltaher, M.A. (2020b), "Weight optimization of axially functionally graded microbeams under buckling and vibration behaviors", *Mech. Based Des. Struct. Mach*., 1-22. https://doi.org/10.1080/15397734.2020.1838298

Abo-Bakr, H.M., Abo-bakr, R.M., Mohamed, S.A. and Eltaher, M.A. (2021), "Multi-objective shape optimization for axially functionally graded microbeams", *Compos. Struct*., **258**, 113370. https://doi.org/10.1016/j.compstruct.2020.113370

Akbaş, Ş.D. (2016), "Forced vibration analysis of viscoelastic nanobeams embedded in an elastic medium", *Smart Struct. Syst*., *Int. J*., **18**(6), 1125-1143. http://dx.doi.org/10.12989/sss.2016.18.6.1125

Alazwari, M.A., Abdelrahman, A.A., Wagih, A., Eltaher, M.A. and Abd-El-Mottaleb, H.E. (2021), "Static analysis of cutout microstructures incorporating the microstructure and surface effects", *Steel Compos. Struct*., *Int. J*., **38**(5), 583-597. https://doi.org/10.12989/scs.2021.38.5.583

Alimirzaei, S., Mohammadimehr, M. and Tounsi, A. (2019), "Nonlinear analysis of viscoelastic micro-composite beam with geometrical imperfection using FEM: MSGT electro-magneto-elastic bending, buckling and vibration solutions", *Struct. Eng. Mech*., *Int. J*., **71**(5), 485-502. https://doi.org/10.12989/sem.2019.71.5.485

Almitani, K.H., Abdelrahman, A.A. and Eltaher, M.A. (2019), "□n forced and free vibrations of cutout squared beams", *Steel Compos. Struct*., *Int. J*., **32**(5), 643-655. https://doi.org/10.12989/scs.2019.32.5.643

Almitani, K.H., Abdelrahman, A.A. and Eltaher, M.A. (2020a), "Influence of the perforation configuration on dynamic behaviors of multilayered beam structure", *Structures*, **28**, 1413-1426. https://doi.org/10.1016/j.istruc.2020.09.055

Almitani, K.H., Abdelrahman, A.A. and Eltaher, M.A. (2020b), "Stability of perforated nanobeams incorporating surface energy effects", *Steel Compos. Struct*., *Int. J*., **35**(4), 555-566. https://doi.org/10.12989/scs.2020.35.4.555

Al-shujairi, M. and Mollamahmutoğlu, Ç. (2018), "Buckling and free vibration analysis of functionally graded sandwich micro-beams resting on elastic foundation by using nonlocal strain gradient theory in conjunction with higher order shear theories under thermal effect", *Compos. Part B*: *Eng*., **154**, 292-312. https://doi.org/10.1016/j.compositesb.2018.08.103

Arani, A.G., Pourjamshidian, M. and Arefi, M. (2017), "Influence of electro-magneto-thermal environment on the wave propagation analysis of sandwich nano-beam based on nonlocal strain gradient theory and shear deformation theories", *Smart Struct. Syst*., *Int. J*., **20**(3), 329-342. http://dx.doi.org/10.12989/sss.2019.23.3.215

Arani, A.G., Pourjamshidian, M. and Arefi, M. (2018), "Non-linear free and forced vibration analysis of sandwich nano-beam with FG-CNTRC face-sheets based on nonlocal strain gradient theory", *Smart Struct. Syst*., *Int. J*., **22**(1), 105-120. https://doi.org/10.12989/sss.2018.22.1.105

Asghar, S., Naeem, M.N., Hussain, M., Taj, M. and Tounsi, A. (2020), "Prediction and assessment of nonlocal natural frequencies of DWCNTs: Vibration analysis", *Comput. Concrete*, *Int. J*., **25**(2), 133-144. https://doi.org/10.12989/cac.2020.25.2.133

Assie, A., Akbaş, Ş.D., Bashiri, A.H., Abdelrahman, A.A. and Eltaher, M.A. (2021), "Vibration response of perforated thick beam under moving load", *Eur. Phys. J. Plus*, **136**(3), 1-15. https://doi.org/10.1140/epjp/s13360-021-01224-2

Balubaid, M., Tounsi, A., Dakhel, B. and Mahmoud, S.R. (2019), "Free vibration investigation of FG nanoscale plate using nonlocal two variables integral refined plate theory", *Comput. Concrete*, *Int. J*., **24**(6), 579-586. https://doi.org/10.12989/cac.2019.24.6.579

Bellal, M., Hebali, H., Heireche, H., Bousahla, A.A., Tounsi, A., Bourada, F., Mahmoud, S.R., Bedia, E.A. and Tounsi, A. (2020), "Buckling behavior of a single-layered graphene sheet resting on viscoelastic medium via nonlocal four-unknown integral model", *Steel Compos. Struct*., *Int. J*., **34**(5), 643-655. https://doi.org/10.12989/scs.2020.34.5.643

Berghouti, H., Adda Bedia, E.A., Benkhedda, A. and Tounsi, A. (2019), "Vibration analysis of nonlocal porous nanobeams made of functionally graded material", *Adv. Nano Res*., *Int. J*., **7**(5), 351-364. https://doi.org/10.12989/anr.2019.7.5.351

Bouafia, K., Kaci, A., Houari, M.S.A., Benzair, A. and Tounsi, A. (2017), "A nonlocal quasi-3D theory for bending and free flexural vibration behaviors of functionally graded nanobeams", *Smart Struct. Syst*., *Int. J*., **19**(2), 115-126. http://dx.doi.org/10.12989/sss.2017.19.2.115

Bourada, F., Bousahla, A.A., Tounsi, A., Bedia, E.A., Mahmoud, S.R., Benrahou, K.H. and Tounsi, A. (2020), "Stability and dynamic analyses of SW-CNT reinforced concrete beam resting on elastic-foundation", *Comput. Concrete*, *Int. J*., **25**(6), 485-495. https://doi.org/10.12989/cac.2020.25.6.485

Bourouina, H., Yahiaoui, R., Sahar, A. and Benamar, M.E.A. (2016), "Analytical modeling for the determination of nonlocal resonance frequencies of perforated nanobeams subjected to temperature-induced loads", *Physica E*: *Low-dimens. Syst. Nanostruct*., **75**, 163-168. http://dx.doi.org/10.1016/j.physe.2015.09.014

Bousahla, A.A., Bourada, F., Mahmoud, S.R., Tounsi, A., Algarni, A., Bedia, E.A. and Tounsi, A. (2020), "Buckling and dynamic behavior of the simply supported CNT-RC beams using an integral-first shear deformation theory", *Comput. Concrete*, *Int. J*., **25**(2), 155-166. https://doi.org/10.12989/cac.2020.25.2.155

Boutaleb, S., Benrahou, K.H., Bakora, A., Algarni, A., Bousahla, A.A., Tounsi, A., Tounsi, A. and Mahmoud, S.R. (2019), "Dynamic analysis of nanosize FG rectangular plates based on simple nonlocal quasi 3D HSDT", *Adv. Nano Res*., *Int. J*., **7**(3), 191-208. https://doi.org/10.12989/anr.2019.7.3.191

Cao, X., Xuan, S., Li, J., Li, Z., Hu, T., Liang, H., Ding, L., Li, B. and Gong, X. (2019), "Magnetic-tunable sound absorber based on micro-perforated magnetorheological elastomer", *Smart Mater. Struct.*, **29**(1), 015024. https://orcid.org/0000-0001-6997-9526

Daikh, A.A., Houari, M.S.A. and Tounsi, A. (2019), "Buckling analysis of porous FGM sandwich nanoplates due to heat conduction via nonlocal strain gradient theory", *Eng. Res. Express*, **1**(1), 015022. https://orcid.org/0000-0002-4666-2750

Daikh, A.A., Drai, A., Bensaid, I., Houari, M.S.A. and Tounsi, A. (2020a), "□n vibration of functionally graded sandwich nanoplates in the thermal environment", *J. Sandw. Struct. Mater.*, 1099636220909790. https://doi.org/10.1177/1099636220909790

Daikh, A.A., Drai, A., Houari M.S.A, and Eltaher, M.A. (2020b), "Static analysis of multilayer nonlocal strain gradient nanobeam reinforced by carbon nanotubes", *Steel Compos. Struct., Int. J.*, **36**(6), 643-656. https://doi.org/10.12989/scs.2020.36.6.64

Daikh, A.A., Houari, M.S.A., Karami, B., Eltaher, M.A., Dimitri, R. and Tornabene, F. (2021a), "Buckling Analysis of CNTRC Curved Sandwich Nanobeams in Thermal Environment", *Appl. Sci.*, **11**(7), 3250. https://doi.org/10.3390/app11073250

Daikh, A.A., Houari, M.S.A. and Eltaher, M.A. (2021b), "A novel nonlocal strain gradient Quasi-3D bending analysis of sigmoid functionally graded sandwich nanoplates", *Compos. Struct.*, **262**, 113347. https://doi.org/10.1016/j.compstruct.2020.113347

Draiche, K., Bousahla, A.A., Tounsi, A., Alwabli, A.S., Tounsi, A. and Mahmoud, S.R. (2019), "Static analysis of laminated reinforced composite plates using a simple first-order shear deformation theory", *Comput. Concrete, Int. J.*, **24**(4), 369-378. https://doi.org/10.12989/cac.2019.24.4.369

Ebrahimi, F. and Barati, M.R. (2016), "Hygrothermal buckling analysis of magnetically actuated embedded higher order functionally graded nanoscale beams considering the neutral surface position", *J. Thermal Stress.*, **39**(10), 1210-1229. https://doi.org/10.1080/01495739.2016.1215726

Ebrahimi, F. and Shafiei, N. (2016), "Application of Eringen's nonlocal elasticity theory for vibration analysis of rotating functionally graded nanobeams", *Smart Struct. Syst., Int. J.*, **17**(5), 837-857. https://doi.org/10.12989/sss.2016.17.5.837

Ebrahimi, F. and Shaghaghi, G.R. (2016), "Thermal effects on nonlocal vibrational characteristics of nanobeams with non-ideal boundary conditions", *Smart Struct. Syst., Int. J.*, **18**(6), 1087-1109. http://dx.doi.org/10.12989/sss.2016.18.6.1087

Ebrahimi, F., Daman, M. and Jafari, A. (2017), "Nonlocal strain gradient-based vibration analysis of embedded curved porous piezoelectric nano-beams in thermal environment", *Smart Struct. Syst., Int. J.*, **20**(6), 709-728. http://dx.doi.org/10.12989/sss.2017.20.6.709

Eglin, M., Eriksson, M.A. and Carpick, R.W. (2006), "Microparticle manipulation using inertial forces", *Appl. Phys. Lett.*, **88**(9), 091913. https://doi.org/10.1063/1.2172401

Eltaher, M.A. and Abdelrahman, A.A. (2020), "Bending behavior of squared cutout nanobeams incorporating surface stress effects", *Steel Compos. Struct., Int. J.*, **36**(2), 143-161. https://doi.org/10.12989/scs.2020.36.2.143

Eltaher, M.A. and Mohamed, N. (2020a), "Nonlinear stability and vibration of imperfect CNTs by Doublet mechanics", *Appl. Mathe. Computat.*, **382**, 125311. https://doi.org/10.1016/j.amc.2020.125311

Eltaher, M.A. and Mohamed, N.A. (2020b), "Vibration of nonlocal perforated nanobeams with general boundary conditions", *Smart Struct. Syst., Int. J.*, **25**(4), 501-514. https://doi.org/10.12989/sss.2020.25.4.501

Eltaher, M.A., Agwa, M.A. and Mahmoud, F.F. (2016), "Nanobeam sensor for measuring a zeptogram mass", *Int. J. Mech. Mater. Des.*, **12**(2), 211-221. https://doi.org/10.1007/s10999-015-9302-5

Eltaher, M.A., Kabeel, A.M., Almitani, K.H. and Abdraboh, A.M. (2018a), "Static bending and buckling of perforated nonlocal size-dependent nanobeams", *Microsyst. Technol.*, **24**(12), 4881-4893. https://doi.org/10.1007/s00542-018-3905-3

Eltaher, M.A., Abdraboh, A.M. and Almitani, K.H. (2018b), "Resonance frequencies of size dependent perforated nonlocal nanobeam", *Microsyst. Technol.*, **24**(9), 3925-3937. https://doi.org/10.1007/s00542-018-3910-6

Eltaher, M.A., Agwa, M. and Kabeel, A. (2018c), "Vibration analysis of material size-dependent CNTs using energy equivalent model", *J. Appl. Computat. Mech.*, **4**(2), 75-86. https://doi.org/10.22055/JACM.2017.22579.1136

Eltaher, M.A., Mohamed, N. and Mohamed, S.A. (2020b), "Nonlinear buckling and free vibration of curved CNTs by doublet mechanics", *Smart Struct. Syst., Int. J.*, **26**(2), 213-226. https://doi.org/10.12989/sss.2020.26.2.213

Eltaher, M.A., □mar, F.A., Abdalla, W.S., Kabeel, A.M. and Alshorbagy, A.E. (2020c), "Mechanical analysis of cutout piezoelectric nonlocal nanobeam including surface energy effects", *Struct. Eng. Mech., Int. J.*, **76**(1), 141-151. https://doi.org/10.12989/sem.2020.76.1.141

Eltaher, M.A., □mar, F.A., Abdraboh, A.M., Abdalla, W.S. and Alshorbagy, A.E. (2020d), "Mechanical behaviors of piezoelectric nonlocal nanobeam with cutouts", *Smart Struct. Syst., Int. J.*, **25**(2), 219-228. https://doi.org/10.12989/sss.2020.25.2.219

Eringen, A.C. (1983), "□n differential equations of nonlocal elasticity and solutions of screw dislocation and surface waves", *J. Appl. Phys.*, **54**(9), 4703-4710. https://doi.org/10.1063/1.332803

Esen, I. (2019a), "Dynamic response of a functionally graded Timoshenko beam on two-parameter elastic foundations due to a variable velocity moving mass", *Int. J. Mech. Sci.*, **153**, 21-35. https://doi.org/10.1016/j.ijmecsci.2019.01.033

Esen, I. (2019b), "Dynamic response of functional graded Timoshenko beams in a thermal environment subjected to an accelerating load", *Eur. J. Mech.-A/Solids*, **78**, 103841. https://doi.org/10.1016/j.euromechsol.2019.103841

Esen, I. (2020), "Dynamics of size-dependant Timoshenko micro beams subjected to moving loads", *Int. J. Mech. Sci.*, **175**, 105501. https://doi.org/10.1016/j.ijmecsci.2020.105501

Esen, I., Abdelrahman, A.A. and Eltaher, M.A. (2020), "Dynamics analysis of timoshenko perforated microbeams under moving loads", *Eng. Comput.*, 1-17. https://doi.org/10.1007/s00366-020-01212-7

Esen, I., Eltaher, M.A. and Abdelrahman, A.A. (2021a), "Vibration response of symmetric and sigmoid functionally graded beam rested on elastic foundation under moving point mass", *Mech. Based Des. Struct. Mach.*, 1-25. https://doi.org/10.1080/15397734.2021.1904255

Esen, I., Özarpa, C. and Eltaher, M.A. (2021b), "Free vibration of a cracked FG microbeam embedded in an elastic matrix and exposed to magnetic field in a thermal environment", *Compos. Struct.*, **261**, 113552. https://doi.org/10.1016/j.compstruct.2021.113552

Esen, I., Daikh, A.A. and Eltaher, M.A. (2021c), "Dynamic response of nonlocal strain gradient FG nanobeam reinforced by carbon nanotubes under moving point load", *Eur. Phys. J. Plus*, **136**(4), 1-22. https://doi.org/10.1140/epjp/s13360-021-01419-7

Esen, I., Abdelrhmaan, A.A. and Eltaher, M.A. (2021d), "Free vibration and buckling stability of FG nanobeams exposed to magnetic and thermal fields", *Eng. Comput.*, 1-20. https://doi.org/10.1007/s00366-021-01389-5

Farajpour, A. and Rastgoo, A. (2017), "Influence of carbon nanotubes on the buckling of microtubule bundles in viscoelastic cytoplasm using nonlocal strain gradient theory",

Results Phys., **7**, 1367-1375. https://doi.org/10.1016/j.rinp.2017.03.038

Ferrari, M., Granik, V.T. and Imam, A. (1997), "Introduction to doublet mechanics", In: *Advances in Doublet Mechanics* (pp. 1-26), Springer, Berlin, Heidelberg.

Ferrari, M., Granik, V.T., Imam, A. and Nadeau, J.C. eds. (2008), *Advances in Doublet Mechanics*, Vol. 45, Springer Science & Business Media.

Ghadiri, M., Rajabpour, A. and Akbarshahi, A. (2017), "Non-linear forced vibration analysis of nanobeams subjected to moving concentrated load resting on a viscoelastic foundation considering thermal and surface effects", *Appl. Mathe. Modell*., **50**, 676-694. https://doi.org/10.1016/j.apm.2017.06.019

Gurtin, M.E. and Murdoch, A.I. (1978), "Surface stress in solids", *Int. J. Solids Struct*., **14**(6), 431-440. https://doi.org/10.1016/0020-7683(78)90008-2

Hamed, M.A., Mohamed, N.A. and Eltaher, M.A. (2020), "Stability buckling and bending of nanobeams including cutouts", *Eng. Comput*., 1-22. https://doi.org/10.1007/s00366-020-01063-2

Hamidi, B.A., Hosseini, S.A., Hayati, H. and Hassannejad, R. (2020), "Forced axial vibration of micro and nanobeam under axial harmonic moving and constant distributed forces via nonlocal strain gradient theory", *Mech. Based Des. Struct. Mach*., 1-15. https://doi.org/10.1080/15397734.2020.1744003

Hashemi, S.H. and Khaniki, H.B. (2018), "Dynamic response of multiple nanobeam system under a moving nanoparticle", *Alexandria Eng. J*., **57**(1), 343-356. https://doi.org/10.1016/j.aej.2016.12.015

Hussain, M., Naeem, M.N., Tounsi, A. and Taj, M. (2019), "Nonlocal effect on the vibration of armchair and zigzag SWCNTs with bending rigidity", *Adv. Nano Res*., *Int. J*., **7**(6), 431-442. https://doi.org/10.12989/anr.2019.7.6.431

Karami, B., Janghorban, M. and Tounsi, A. (2019a), "Galerkin's approach for buckling analysis of functionally graded anisotropic nanoplates/different boundary conditions. *Eng. Comput*., **35**(4), 1297-1316. https://doi.org/10.1007/s00366-018-0664-9

Karami, B., Janghorban, M. and Tounsi, A. (2019b), "□n pre-stressed functionally graded anisotropic nanoshell in magnetic field", *J. Brazil. Soc. Mech. Sci. Eng*., **41**(11), 1-17. https://doi.org/10.1007/s40430-019-1996-0

Kim, T., Park, I. and Lee, U. (2017), "Forced vibration of a Timoshenko beam subjected to stationary and moving loads using the modal analysis method", *Shock Vib*., 3924921. https://doi.org/10.1155/2017/3924921

Kim, H.S., Kim, S.R., Kim, B.K., Ma, P.S. and Seo, Y.H. (2020), "Sound transmission loss of multi-layered infinite micro-perforated plates", *J. Acoust. Soc. Am*., **147**(1), 508-515. https://doi.org/10.1121/10.0000600

Koiter, W.T. (1964), "Couple stresses in the theory of elasticity", *Proc. Koninklijke Nederl Akaad van Wetensch*, **67**, p. 20. https://hal.archives-ouvertes.fr/hal-00852443

Li, L. and Hu, Y. (2016), "Nonlinear bending and free vibration analyses of nonlocal strain gradient beams made of functionally graded material", *Int. J. Eng. Sci*., **107**, 77-97. https://doi.org/10.1016/j.ijengsci.2016.07.011

Li, Y. and Li, M. (2020), "Dynamic analysis of rotating double-tapered cantilever Timoshenko nano-beam using the nonlocal strain gradient theory", *Mathe. Methods Appl. Sci*., **43**(15), 9206-9222. https://doi.org/10.1002/mma.6616

Li, C., Shen, Q., Yao, L. and Li, S. (2015a), "Lateral bending vibration of nanoscale ultra-thin beams using a semi-continuum model", *J. Computat. Theor. Nanosci*., **12**(9), 2507-2514. https://doi.org/10.1166/jctn.2015.4056

Li, C., Chen, L. and Shen, J.P. (2015b), "Vibrational responses of micro/nanoscale beams: size-dependent nonlocal model analysis and comparisons", *J. Mech*., **31**(1), 7-19. https://doi.org/10.1017/jmech.2014.50

Li, L., Li, X. and Hu, Y. (2016), "Free vibration analysis of nonlocal strain gradient beams made of functionally graded material", *Int. J. Eng. Sci*., **102**, 77-92. https://doi.org/10.1016/j.ijengsci.2016.02.010

Li, C., Lai, S.K. and Yang, X. (2019), "□n the nano-structural dependence of nonlocal dynamics and its relationship to the upper limit of nonlocal scale parameter", *Appl. Mathe. Modell*., **69**, 127-141. https://doi.org/10.1016/j.apm.2018.12.010

Lim, C.W., Zhang, G. and Reddy, J.N. (2015), "A higher-order nonlocal elasticity and strain gradient theory and its applications in wave propagation", *J. Mech. Phys. Solids*, **78**, 298-313. https://doi.org/10.1016/j.jmps.2015.02.001

Lou, P., Dai, G.L. and Zeng, Q.Y. (2007), "Dynamic analysis of a Timoshenko beam subjected to moving concentrated forces using the finite element method", *Shock Vib*., **14**(6), 459-468.

Lu, L., Guo, X. and Zhao, J. (2018), "□n the mechanics of Kirchhoff and Mindlin plates incorporating surface energy", *Int. J. Eng. Sci*., **124**, 24-40. https://doi.org/10.1016/j.ijengsci.2017.11.020

Lu, L., She, G.L. and Guo, X. (2021), "Size-dependent postbuckling analysis of graphene reinforced composite microtubes with geometrical imperfection", *Int. J. Mech. Sci*., **199**, 106428. https://doi.org/10.1016/j.ijmecsci.2021.106428

Luschi, L. and Pieri, F. (2014), "An analytical model for the determination of resonance frequencies of perforated beams", *J. Micromech. Microeng*., **24**(5), 055004. https://doi.org/10.1088/0960-1317/24/5/055004

Ma, H.M., Gao, X.L. and Reddy, J.N. (2008), "A microstructure-dependent Timoshenko beam model based on a modified couple stress theory", *J. Mech. Phys. Solids*, **56**(12), 3379-3391. https://doi.org/10.1016/j.jmps.2008.09.007

Mahmoud, F.F., Eltaher, M.A., Alshorbagy, A.E. and Meletis, E.I. (2012), "Static analysis of nanobeams including surface effects by nonlocal finite element", *J. Mech. Sci. Technol*., **26**(11), 3555-3563. https://doi.org/10.1007/s12206-012-0871-z

Matouk, H., Bousahla, A.A., Heireche, H., Bourada, F., Bedia, E.A., Tounsi, A., Mahmoud, S.R., Tounsi, A. and Benrahou, K.H. (2020), "Investigation on hygro-thermal vibration of P-FG and symmetric S-FG nanobeam using integral Timoshenko beam theory", *Adv. Nano Res*., *Int. J*., **8**(4), 293-305. https://doi.org/10.12989/anr.2020.8.4.293

Mindlin, R.D. (1965), "Second gradient of strain and surface-tension in linear elasticity", *Int. J. Solids Struct*., **1**(4), 417-438. https://doi.org/10.1016/0020-7683(65)90006-5

Mohamed, N., Eltaher, M.A., Mohamed, S.A. and Seddek, L.F. (2019), "Energy equivalent model in analysis of postbuckling of imperfect carbon nanotubes resting on nonlinear elastic foundation", *Struct. Eng. Mech*., *Int. J*., **70**(6), 737-750. https://doi.org/10.12989/sem.2019.70.6.737

Mohamed, N., Mohamed, S.A. and Eltaher, M.A. (2020), "Buckling and post-buckling behaviors of higher order carbon nanotubes using energy-equivalent model", *Eng. Comput*., 1-14. https://doi.org/10.1007/s00366-020-00976-2

Mouffoki, A., Bedia, E.A., Houari, M.S.A., Tounsi, A. and Mahmoud, S.R. (2017), "Vibration analysis of nonlocal advanced nanobeams in hygro-thermal environment using a new two-unknown trigonometric shear deformation beam theory", *Smart Struct. Syst*., *Int. J*., **20**(3), 369-383. http://dx.doi.org/10.12989/sss.2017.20.3.369

Nix, W.D. and Gao, H. (1998), "Indentation size effects in crystalline materials: a law for strain gradient plasticity", *J. Mech. Phys. Solids*, **46**(3), 411-425. https://doi.org/10.1016/S0022-5096(97)00086-0

Özarpa, C. and Esen, I. (2020), "Modelling the dynamics of a nanocapillary system with a moving mass using the non-local

strain gradient theory", *Mathe. Methods Appl. Sci.* https://doi.org/10.1002/mma.6812

Pourseifi, M., Rahmani, □. and Hoseini, S.A.H. (2015), "Active vibration control of nanotube structures under a moving nanoparticle based on the nonlocal continuum theories", *Meccanica*, **50**(5), 1351-1369. https://doi.org/10.1007/s11012-014-0096-6

Reddy, J.N. (2007), "Nonlocal theories for bending, buckling and vibration of beams", *Int. J. Eng. Sci.*, **45**(2-8), 288-307. https://doi.org/10.1016/j.ijengsci.2007.04.004

Reddy, J.N. (2017), *Energy principles and variational methods in applied mechanics*, John Wiley & Sons.

Rouabhia, A., Chikh, A., Bousahla, A.A., Bourada, F., Heireche, H., Tounsi, A., Kouider Halim, B., Tounsi, A. and Al-Zahrani, M.M. (2020), "Physical stability response of a SLGS resting on viscoelastic medium using nonlocal integral first-order theory", *Steel Compos. Struct., Int. J.*, **37**(6), 695-709. https://doi.org/10.12989/scs.2020.37.6.695

Roudbari, M.A., Jorshari, T.D., Arani, A.G., Lü, C. and Rabczuk, T. (2020), "Transient responses of two mutually interacting single-walled boron nitride nanotubes induced by a moving nanoparticle", *Eur. J. Mech.-A/Solids*, 103978. https://doi.org/10.1016/j.euromechsol.2020.103978

Salvetat, J.P., Briggs, G.A.D., Bonard, J.M., Bacsa, R.R., Kulik, A.J., Stöckli, T., Burnham, N.A. and Forró, L. (1999), "Elastic and shear moduli of single-walled carbon nanotube ropes", *Phys. Rev. Lett.*, **82**(5), 944. https://doi.org/10.1103/PhysRevLett.82.944

Semmah, A., Heireche, H., Bousahla, A.A. and Tounsi, A. (2019), "Thermal buckling analysis of SWBNNT on Winkler foundation by non local FSDT", *Adv. Nano Res., Int. J.*, **7**(2), 89-98. https://doi.org/10.12989/anr.2019.7.2.089

She, G.L. (2020), "Wave propagation of FG polymer composite nanoplates reinforced with GNPs", *Steel Compos. Struct., Int. J.*, **37**(1), 27-35. https://doi.org/10.12989/scs.2020.37.1.027

She, G.L., Liu, H.B. and Karami, B. (2021), "Resonance analysis of composite curved microbeams reinforced with graphene nanoplatelets", *Thin-Wall. Struct.*, **160**, 107407. https://doi.org/10.1016/j.tws.2020.107407

Shen, J.P. and Li, C. (2017), "A semi-continuum-based bending analysis for extreme-thin micro/nano-beams and new proposal for nonlocal differential constitution", *Compos. Struct.*, **172**, 210-220. https://doi.org/10.1016/j.compstruct.2017.03.070

Shen, J.P., Li, C., Fan, X.L. and Jung, C.M. (2017), "Dynamics of silicon nanobeams with axial motion subjected to transverse and longitudinal loads considering nonlocal and surface effects", *Smart Struct. Syst., Int. J.*, **19**(1), 105-113. http://dx.doi.org/10.12989/sss.2017.19.1.105

Shen, J.P., Wang, P.Y., Li, C. and Wang, Y.Y. (2019), "New observations on transverse dynamics of microtubules based on nonlocal strain gradient theory", *Compos. Struct.*, **225**, 111036. https://doi.org/10.1016/j.compstruct.2019.111036

Shen, J.P., Wang, P.Y., Gan, W.T. and Li, C. (2020), "Stability of vibrating functionally graded nanoplates with axial motion based on the nonlocal strain gradient theory", *Int. J. Struct. Stabil. Dyn.*, **20**(08), 2050088. https://doi.org/10.1142/S0219455420500881

Şimşek, M. (2010), "Dynamic analysis of an embedded microbeam carrying a moving microparticle based on the modified couple stress theory", *Int. J. Eng. Sci.*, **48**(12), 1721-1732. https://doi.org/10.1016/j.ijengsci.2010.09.027

Thai, H.T. (2012), "A nonlocal beam theory for bending, buckling, and vibration of nanobeams", *Int. J. Eng. Sci.*, **52**, 56-64. https://doi.org/10.1016/j.ijengsci.2011.11.011

Thai, H.T. and Vo, T.P. (2012), "A nonlocal sinusoidal shear deformation beam theory with application to bending, buckling, and vibration of nanobeams", *Int. J. Eng. Sci.*, **54**, 58-66. https://doi.org/10.1016/j.ijengsci.2012.01.009

Uzun, B., Kafkas, U. and Yaylı, M.Ö. (2020), "Free vibration analysis of nanotube based sensors including rotary inertia based on the Rayleigh beam and modified couple stress theories", *Microsyst. Technol.*, **27**, 1913-1923. https://doi.org/10.1007/s00542-020-04961-z

Wu, Y., Zhang, X., Leung, A.Y.T. and Zhong, W. (2006), "An energy-equivalent model on studying the mechanical properties of single-walled carbon nanotubes", *Thin-Wall. Struct.*, **44**(6), 667-676. https://doi.org/10.1016/j.tws.2006.05.003

Xie, K., Wang, Y. and Fu, T. (2020), "Nonlinear vibration analysis of third-order shear deformable functionally graded beams by a new method based on direct numerical integration technique", *Int. J. Mech. Mater. Des.*, **16**(4), 839-855. https://doi.org/10.1007/s10999-020-09493-y

Yao, L.Q., Ji, C.J., Shen, J.P. and Li, C. (2020), "Free vibration and wave propagation of axially moving functionally graded Timoshenko microbeams", *J. Brazil. Soc. Mech. Sci. Eng.*, **42**(3), 1-14. https://doi.org/10.1007/s40430-020-2206-9

Yaylı, M.Ö. (2015), "Stability analysis of gradient elastic microbeams with arbitrary boundary conditions", *J. Mech. Sci. Technol.*, **29**(8), 3373-3380. https://doi.org/10.1007/s12206-015-0735-4

Yayli, M.Ö. (2016), "Buckling analysis of a microbeam embedded in an elastic medium with deformable boundary conditions", *Micro Nano Lett.*, **11**(11), 741-745. https://doi.org/10.1049/mnl.2016.0257

Yayli, M.Ö. (2018a), "Torsional vibrations of restrained nanotubes using modified couple stress theory", *Microsyst. Technol.*, **24**(8), 3425-3435. https://doi.org/10.1007/s00542-018-3735-3

Yayli, M.Ö. (2018b), "□n the torsional vibrations of restrained nanotubes embedded in an elastic medium", *J. Brazil. Soc. Mech. Sci. Eng.*, **40**(9), 1-12. https://doi.org/10.1007/s40430-018-1346-7

Yayli, M.Ö. (2018c), "An efficient solution method for the longitudinal vibration of nanorods with arbitrary boundary conditions via a hardening nonlocal approach", *J. Vib. Control*, **24**(11), 2230-2246. https://doi.org/10.1177/1077546316684042

Yayli, M.Ö. (2020), "A solution method for longitudinal vibrations of functionally graded nanorods", *Int. J. Eng. Appl. Sci.*, **12**(2), 78-87. https://doi.org/10.24107/ijeas.782419

Yaylı, M.Ö., Uzun, B. and Deliktaş, B. (2021), "Buckling analysis of restrained nanobeams using strain gradient elasticity", *Waves Random Complex Media*, 1-20. https://doi.org/10.1080/17455030.2020.1871112

CC